2024

ANOMALY MAPPING OF HEAVY AND LIGHT RARE EARTH ELEMENTS IN CENTRAL UPPER PENINSULA OF MICHIGAN USING GEOSTATISTICS AND FRACTAL ANALYSIS

Sunday Joseph
Michigan Technological University, sundayj@mtu.edu

ANOMALY MAPPING OF HEAVY AND LIGHT RARE EARTH ELEMENTS IN CENTRAL UPPER PENINSULA OF MICHIGAN USING GEOSTATISTICS AND FRACTAL ANALYSIS

By

Sunday Joseph

A REPORT

Submitted in partial fulfillment of the requirements for the degree of

MASTER OF SCIENCE

In Geophysics

MICHIGAN TECHNOLOGICAL UNIVERSITY

2024

This report has been approved in partial fulfillment of the requirements for the Degree of MASTER OF SCIENCE in Geophysics.

Department of Geological and Mining Engineering and Sciences

Report Advisor:	*Dr. Snehamoy Chatterjee*
Committee Member:	*Dr. Luke Bowman*
Committee Member:	*Dr. Chad Deering*
Department Chair:	*Dr. Aleksey Smirnov*

Table of Contents

List of Figures

List of Tables

Acknowledgements

To my mom, and in loving memory of my dad.

To Dr. Snehamoy Chatterjee, Dr. Luke Bowman, Dr. Radwin Askari, Dr. Chad Deering, and Dr. Isi Awaah, thank you so much for your incredible support during my time at Michigan Tech.

And to my wife Ejodamen, and kids Michelle, Nathan, Ariella, and Nadia, thank you all for your patience and love during my absence.

List of Abbreviations

C-A	concentration area
CBA	complete bouguer anomaly
Ce	Cerium
Dy	Dysprosium
Er	Erbium
Eu	Europium
Ho	Holmium
HREE	heavy rare earth elements
La	Lanthanum
LREE	light rare earth elements
Lu	Lutetium
Nd	Neodymium
ppm	parts per million
Pr	Praseodymium
Pm	Promethium
REE	rare earth elements
RMS	root mean square
Sc	Scandium
Sm	Samarium
Tb	Terbium
Tm	Thulium
Y	Yttrium
Yb	Ytterbium
EV	electric vehicle

Abstract

Rare earth elements (REEs) have gained significant global importance due to their critical role in supporting the transition towards reduced carbon emissions through industrial applications. REEs serve as essential raw materials for various critical components in modern infrastructure, defense systems, and technological advancements. Geochemical and geophysical data are pivotal in assessing the potential of REEs. Geochemical data provide direct insights into the elemental composition of rocks and soils, offering valuable information on the potential presence and dispersion of REEs. However, the complex geological processes that influence the distribution of REEs often exhibit intricate spatial patterns that may not be fully captured by geochemical data alone. Geophysical data, such as gravity and magnetic data, offer indirect but complementary insights into subsurface geological structures and mineral potential. The integration of geochemical, gravity, and magnetic data can aid in identifying exploration targets with increased confidence levels. While each data source individually provides valuable information, their combination allows for the identification of areas where multiple anomalies coincide, indicating a higher likelihood of mineralization. This approach helps reduce exploration uncertainties by prioritizing targets that exhibit consistent characteristics across various datasets, thereby enhancing the chances of discovering economically viable REE reserves.

This study aims to investigate the geochemical anomalies of REEs in Central Upper Michigan by employing geostatistics and fractal analysis to integrate geochemical, gravity, and magnetic data to quantify and map REEs anomalies. Both the heavy and light REEs (HREEs and LREEs) were mapped, integrating with gravity and magnetic data using a multivariate geostatistical method called cokriging. Cokriging utilized the spatial correlation and cross-correlation among these data types to provide more insightful predictions compared to solely relying on the geochemical dataset. Fractal modeling, which has proven to be a powerful tool in geological mapping for anomalous deposits, was utilized in this study. By leveraging the fractal characteristics of mineral deposit dispersion and the related geochemical trends, this approach was able to identify potential exploration zones. The concentration-Area (C-A) log-log plots of the HREEs and LREEs were generated, and their thresholds were subsequently identified using the segmented linear method. The fundamental premise of C-A fractal modeling is based on the observation that mineralization processes frequently result in patterns of element concentrations that exhibit fractal characteristics. These patterns can be analyzed to distinguish between the baseline (typical levels found in the earth's crust) and anomalies (elevated concentrations indicative of mineral deposits). Results from this study clearly show the anomaly distributions of both the HREEs and LREEs across the study area. Combining geochemical information with additional datasets results in a more thorough comprehension of subsurface circumstances, which is essential for precise anomaly mapping. The collaboration of these datasets enables a strong analysis, ultimately leading to a more dependable identification of possible mineral deposits and geological characteristics.

1 Introduction

Rare earth elements (REEs) were initially identified in the year 1787 by Karl Axel Arrhenius, a Swedish Army Lieutenant, who retrieved the dark mineral ytterbite (subsequently renamed gadolinite) from a mine containing feldspar and quartz situated near the village of Ytterby, Sweden (Weeks and Leicester, 1968). REEs are a group of 17 chemically similar elements found in the periodic table. This category consists of the 15 lanthanides, which range from lanthanum (La) at atomic number 57 to lutetium (Lu) at atomic number 71, as well as scandium (Sc) and yttrium (Y). These two elements are included due to their presence in the same mineral matrices and comparable chemical behaviors. Despite being termed "rare earth," these elements are quite abundant in the Earth's crust, with cerium, for example, being more plentiful than copper. Nevertheless, the main challenge lies not in their abundance but in their scattered distribution, making it economically and technically challenging to concentrate and extract them. REEs, previously a little-known category of metals, has gained global importance due to their role in industrial uses that support a worldwide shift towards lower carbon emissions. The high-tech sector is projected to see ongoing expansion, driving the need for REE, especially in technologies aimed at reducing carbon output. These elements are essential for producing advanced magnets and are key components in a variety of popular electronics and certain military uses. REE compounds are known for their high melting and boiling points, rendering them crucial and irreplaceable in numerous electronic, optical, magnetic, and catalytic applications (African Natural Resources Centre [ANRC], 2021).

Initially, the integration of diverse data sources enables a more exhaustive comprehension of geological processes and mineralization mechanisms. Geochemical data furnish direct insights into the elemental composition of rocks and soils, thereby shedding light on the potential existence and dispersion of REEs. Nevertheless, the geological processes governing REE distribution often manifest intricate spatial patterns that may not be completely captured by geochemical data in isolation. Conversely, gravity and magnetic data supply indirect yet supplementary insights into subsurface geological structures and mineral deposits. Through the synthesis of these datasets, scholars can corroborate interpretations and enhance geological frameworks, culminating in a more robust grasp of REEs distribution patterns. Moreover, the integration of geochemical, gravity, and magnetic data facilitates the delineation of exploration targets with heightened levels of confidence. Although each data source in isolation offers valuable insights, their amalgamation enables the pinpointing of regions where multiple anomalies intersect, suggesting a greater probability of mineralization. This method mitigates exploration uncertainties by prioritizing targets that demonstrate consistent characteristics across diverse datasets, thereby enhancing the likelihood of discovering economically feasible REEs reserves.

Additionally, the originality of this study is evident in its deviation from the conventional dependence solely on magnetic data for mapping REEs deposits. While magnetic surveys are widely utilized in mineral prospecting due to their sensitivity to magnetic minerals linked to REEs -rich formations, they do have constraints, especially in regions with

intricate geological conditions or where magnetic anomalies are faint or equivocal. By integrating geochemical data, which directly reflect the elemental composition of rocks and soils, alongside gravity and magnetic data, researchers can overcome these limitations and achieve a more holistic understanding of REE distribution. This methodological innovation offers several advantages over conventional approaches. Firstly, it enhances the accuracy and resolution of REEs exploration maps by incorporating multiple lines of evidence. Secondly, it improves the efficiency of exploration campaigns by focusing efforts on targets with the highest potential for mineralization. Finally, it contributes to a more sustainable and environmentally responsible approach to mineral exploration by reducing the need for extensive drilling and fieldwork through targeted prospectivity mapping.

1.1 Occurrence of rare earth elements

In the natural environment, REEs do not occur in their pure metallic form like gold, copper, and silver due to their high reactivity. Instead, they are commonly found collectively in various mineral ores as either minor or major components. While REE can be present in a variety of minerals such as silicates, carbonates, oxides, and phosphates, they do not easily integrate into most mineral structures and are restricted to specific geological settings. Bastnaesite, monazite, loparite, and ion-adsorption clays in lateritic deposits are the primary sources of economically viable REEs minerals (Balaram, 2019).

REEs are typically found in rock-forming minerals in the form of trivalent cations within various compounds such as carbonates, oxides, phosphates, and silicates (Mason and Moore, 1982). Carbonatites, distinctive igneous formations, represent the predominant reservoir for light REEs (LREEs), whereas bastnäsite deposits in mountainous regions encompass both LREEs and heavy REEs (HREE). Monazite sands, identified in alluvial deposits, exhibit high concentrations of thorium and REEs. Xenotime deposits, albeit less prevalent, serve as a crucial reservoir of HREE (Chen, Honghui, Bai, & Jiang, 2017).

1.2 Classification of rare earth elements

REEs are commonly classified into light and heavy groups, with scandium unclassified (Henderson, 1996). The classification of REEs into LREEs and HREEs is determined by their atomic weights and unique magnetic, electrical, and optical characteristics, which influence their specific functionalities and economic significance. LREEs, such as lanthanum, cerium, and praseodymium, are more prevalent in the Earth's crust and therefore less costly compared to their heavier counterparts. LREEs consist of lanthanum (La), cerium (Ce), praseodymium (Pr), neodymium (Nd), promethium (Pm), samarium (Sm), europium (Eu), and gadolinium (Gd), which are renowned for their larger ionic radii. In contrast, HREEs comprise elements starting from terbium (Tb), dysprosium (Dy), holmium (Ho), erbium (Er), thulium (Tm), ytterbium (Yb), and lutetium (Lu), in addition to yttrium (Y), known for their smaller ionic radii and often higher economic value because of their rarity and specific applications in technology and industry. These elements are primarily employed in industrial applications like petroleum refining, glass

production, and ceramics manufacturing, where their attributes contribute to enhanced efficiency and performance (Rudnick and Gao, 2003).

1.3 Importance of rare earth elements

According to the United States Geological Survey (USGS) news release "Going Critical," (American Geosciences Institute, n.d.) "REE are necessary components of more than 200 products across a wide range of applications, especially high-tech consumer products, such as cellular telephones, computer hard drives, electric and hybrid vehicles, and flat-screen monitors and televisions. Significant defense applications include electronic displays, guidance systems, lasers, and radar and sonar systems. Although the amount of REEs used in a product may not be a significant part of that product by weight, value, or volume, the REE can be necessary for the device to function. For example, magnets made of REEs often represent only a small fraction of the total weight, but without them, the spindle motors and voice coils of desktops and laptops would not be possible".

REEs are characterized by their outstanding electronic, optical, and magnetic properties, which render them indispensable in various applications. Electronically, they play a crucial role in the production of high-tech devices by enhancing battery life and electronic display colors. Optically, elements like europium and terbium are utilized to create vivid colors on the screens of smartphones and televisions. Magnetically, REEs such as neodymium are essential in manufacturing high-strength permanent magnets used in wind turbines, electric vehicle motors, and different computer hardware. These properties are not only distinctive but also cannot be substituted with current technology, emphasizing the significance of REEs in the advancement of modern technology and the promotion of renewable energy and more efficient electronic devices. Their extensive use in critical and strategic technologies makes ensuring a reliable supply of REEs a matter of both economic and national security concern for numerous nations, driving efforts to discover more sustainable and less geopolitically vulnerable sources. The occurrence of REEs has predominantly been derived from bedrock and regolith-based ion-adsorption deposits (IADs) formed because of the weathering process of igneous rocks (Borst et al., 2020).

The significance of REEs in modern technology and industry is profound because of their distinct characteristics, which render them essential in a wide range of applications. Within the realm of consumer electronics, REEs are crucial for manufacturing high-performance magnets, batteries, and alloys necessary for the functionality of computers, smartphones, and other digital devices. For instance, europium and terbium are essential for creating vivid screens on smartphones, while neodymium magnets improve the audio quality of headphones and speakers. In the field of sustainable technology and energy, REEs like neodymium and dysprosium are employed in the production of strong magnets vital for wind turbines and electric vehicles, playing a critical role in the shift towards renewable energy sources that are crucial for mitigating carbon emissions and addressing climate change. Electric vehicles were formerly considered a luxury that was out of reach for many due to high costs, but the pressing global imperative to diminish carbon emissions has transformed EVs into a necessity. This shift is poised to gradually supplant

traditional internal combustion engine (ICE) vehicles and those dependent on fossil fuels. The adoption of electric vehicles is expected to surge in the upcoming two decades as they emerge as the primary feasible option to displace fossil fuel-powered vehicles. Consequently, this transition in technology alone will propel REE demand to unparalleled heights. The surge in EV utilization will lead to a fresh surge in demand for rare earth elements, particularly Neodymium (Nd) and Dysprosium (Dy), given their prevalent use in electric vehicle motor magnets and batteries (ANRC, 2021).

The defense and aerospace industries also heavily rely on REEs for the development of advanced weaponry and equipment, such as precision-guided munitions, night-vision goggles, and sophisticated communication systems; REEs aid in the downsizing of electronic devices, enhancing their efficiency and dependability. Moreover, in the healthcare sector, gadolinium is pivotal in magnetic resonance imaging (MRI) for improved imaging precision, and other REEs are utilized in the creation of medications for cancer treatment and surgical tools, highlighting their importance not only in cutting-edge technologies but also in essential healthcare solutions (King, n.d.). Furthermore, LREEs play a vital role in the manufacturing of automotive catalytic converters, serving as catalysts to reduce harmful emissions. On the contrary, HREEs, including elements like europium, terbium, and dysprosium, are present in lower quantities and are utilized in more specialized and high-value sectors. These heavier elements are crucial for the development of robust permanent magnets essential for high-performance motors, advanced electronics, and critical military equipment. The scarcity and specialized uses of HREEs result in their high demand, rendering them valuable and strategically significant in global markets. This differentiation not only emphasizes the varied industrial applications of REEs but also stresses the strategic importance of effectively managing their supply chains, considering the differing abundance and essential roles of these crucial minerals.

The United States Geological Survey (USGS) news release "Going Critical" also posited that in 1993, a significant portion of global REEs production was distributed among various countries. Specifically, China, the United States, Australia, Malaysia, and India accounted for different percentages of production. Over time, however, the dominance of China in the global REEs market increased significantly. By 2011, China had a staggering 97 percent share of world production, reflecting a substantial shift in the industry. The Chinese government's interventions, such as altering production and export quotas, played a crucial role in shaping the dynamics of the REEs market during this period. Furthermore, restrictions were imposed on the export activities of Chinese and Sino-foreign joint-venture companies, further consolidating China's position as a key player in the global REEs market.

At present, more than 95% of the global REEs are extracted from two categories of ore deposits located in China (Humphries, 2010, Long et al., 2010). The primary deposit, Bayan Obo, which is recognized as the largest REE deposit, constitutes a high-grade, igneous-related carbonatite deposit responsible for contributing 80% of the world's Light Rare Earth Elements (LREEs) (U.S. Geological Survey, 2011, Kynicky et al., 2012, Verplanck et al., 2014). Nonetheless, typical of this deposit type, it exhibits low levels of

HREEs. Conversely, the ion-adsorption clay-type deposits situated in South China, although relatively small and low in grade, dominate the HREE market due to their significant enrichment in HREEs and the efficient extraction and processing methods employed, resulting in minimal costs (Long et al., 2010, Kynicky et al., 2012). According to Emsbo et al. (2014), sedimentary phosphate deposits may also play a crucial role in solving the global REEs crisis, suggesting an alternative source that might supplement the existing supply from traditional mining methods.

1.4 Exploration of rare earth elements

Exploration for HREEs and LREEs utilizes a range of methodologies, such as geological mapping, geochemical analysis, remote sensing, geophysical surveys, and drilling, with the aim of identifying geological formations and deposits enriched in REEs (Booysen et al., 2019). Researchers are presently involved in various research avenues for HREEs and LREEs exploration and prospectivity mapping (Khalajmasoumi et al., 2017). Geochemical surveys entail extensive examination of soil, rock, and water samples to determine areas with elevated REEs concentrations (Rodríguez Alfaro et al., 2017). Remote sensing methods, such as hyperspectral imaging and satellite imagery analysis, are employed to identify surface mineralogy linked to REEs deposits, enabling efficient mapping of extensive regions (Bedini, 2017). Geophysical surveys, including magnetic and electromagnetic techniques, aid in identifying subsurface geological structures that may contain REEs deposits, providing crucial data for prospectivity mapping (Farahbakhsh et al., 2023). Furthermore, advancements in analytical techniques like mass spectrometry and X-ray fluorescence allow for more precise and effective analysis of REEs levels in geological specimens (Balaram, 2023).

However, several constraints impede REEs exploration endeavors. The intricate nature of geological processes responsible for REEs concentration poses difficulties in accurately predicting their distribution, particularly for prospectivity mapping (Dushyantha & Madhubhashani, 2020). Additionally, the substantial financial investments and access to remote or politically sensitive areas required for REEs exploration and prospectivity mapping can be restrictive for numerous researchers and companies. Environmental apprehensions regarding the extraction and processing of REEs ores, encompassing habitat degradation and pollution, present significant obstacles that necessitate attention. Moreover, market fluctuations driven by technological advancements, economic factors, and geopolitical dynamics can impact investment decisions and the feasibility of exploration projects. Nonetheless, continuous research and progress in exploration techniques offer encouraging prospects for the identification and sustainable extraction of HREEs and LREEs. These endeavors ensure the ongoing contribution of REEs to technological advancements and economic growth while addressing environmental and economic challenges.

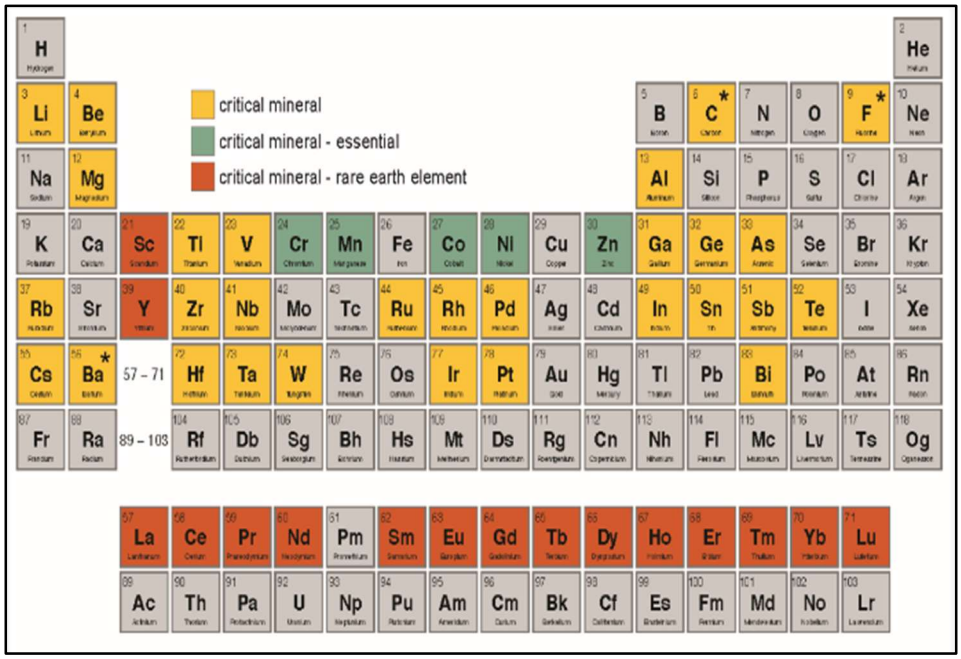

Figure 1. 1 Periodic table highlighting rare earth elements (Jenkins, Musgrove, & White, 2023).

2 Geology of rare earth elements

According to the Virginia Department of Energy (n.d.), most REEs are abundant in the earth's crust, although they are rarely found in their pure metal form. Lanthanum, for example, has an average concentration of 31 parts per million (ppm) in the Earth's crust, slightly higher than copper at 28 ppm (Rudnick and Gao, 2003). On the other hand, thulium, the least abundant naturally occurring rare earth element, has an average concentration of 0.30 ppm, still significantly higher than silver at 0.053 ppm. The relatively large size and charge balance properties of rare earth elements in magmatic systems generally prevent their incorporation into common rock-forming minerals such as feldspars, quartz, amphiboles, and micas. As a result, rare earth elements tend to accumulate in rocks formed by magmas that have undergone significant fractionation. These rocks include alkaline and silicic igneous complexes, pegmatites, felsic volcanics, and carbonatites. Due to their similar ionic sizes, thorium and uranium are often found in association with rare earth elements. Additionally, high-temperature hydrothermal fluids, particularly those rich in chlorine, fluorine, and lithium, can also transport rare earth elements. Economically viable deposits of rare earth elements are typically located in magmatic systems, magmatic magnetite-hematite, or iron oxide-copper-gold (IOCG) deposits, heavy mineral placers, and chemical weathering zones within ion-adsorption clay deposits (USGS, 2020).

The formation and distribution of REEs in geogenic settings are influenced by intricate geochemical and geological processes, with their concentration and extraction linked to their presence in specific rock types. Particularly, primary magmatic activities play a crucial role in concentrating REEs in distinct igneous rocks like carbonatites and peralkaline formations. Carbonatites, which are uncommon igneous rocks mainly composed of carbonate minerals, act as primary hosts for REEs. These rocks signify highly evolved magmatic events, where volatile-rich magma aids in the solubility and mobility of REEs, leading to their precipitation within carbonate-rich matrices. Another important host for REEs is peralkaline igneous rocks, characterized by an excess of alkalis compared to aluminum. These rocks form in environments where partial melting of the Earth's mantle or extreme magma differentiation results in the enrichment of alkalis and REEs. This geochemical setting favors the development of REEs -rich minerals like eudialyte in nepheline syenites or xenotime in granites. Furthermore, hydrothermal processes contribute to the secondary concentration of REEs in veins or by altering host rocks such as quartz-rich rocks, carbonates, and phosphates. Heat-mobilized hydrothermal fluids dissolve and transport REEs, depositing them in mineralized veins within host rocks. This mechanism leads to the creation of REE-rich minerals like bastnäsite, monazite, and xenotime embedded in hydrothermally altered rocks.

In sedimentary contexts, placer deposits act as secondary concentrators of REEs, forming in river and beach sands where water's sorting action concentrates heavy and chemically resistant minerals. REE-bearing minerals such as monazite, xenotime, and allanite are present in these deposits, having been eroded from their primary sources and transported by water. In tropical and subtropical climates, weathering processes contribute to the development of lateritic and ion-adsorption clay deposits. Intense chemical weathering

enhances the leaching of non- REEs minerals from rocks, enriching the soil with REEs. These REEs bind to clay minerals in the soil, forming ion-adsorption deposits rich in HREEs. These deposits are significant due to their relatively straightforward and cost-effective extraction methods.

2.1 Geology settings of the area

In the regions of central Upper Michigan and Northeastern Wisconsin, REEs can be found within a geological context characterized by ancient Precambrian rocks that are part of the Canadian Shield. This area is renowned for its intricate geological past, featuring rock formations that date back over one billion years, such as granites, rhyolites, and basalts, as well as metamorphic rocks like gneiss and schist, which serve as indicators of the region's dynamic tectonic history. The mineral composition of the region indicates the potential presence of REEs deposits in conjunction with alkaline igneous complexes and occurrences of carbonatite. Central Upper Michigan, with its rich geological history and diversity, presents a significant potential for the occurrence of REEs deposits. The geological characteristics of Northeastern Wisconsin, situated within the Superior Upland of the Great Lakes area, consist of ancient Precambrian crystalline rocks overlain by Paleozoic sedimentary layers. These foundational rocks, which are primarily granitic and volcanic in nature, establish the underlying structure of the region. Above these, sedimentary rocks deposited in shallow seas during the Paleozoic era are present, such as dolostones, limestones, and sandstones. Additionally, the landscape is marked by glacial deposits from the most recent Ice Age, which have a significant impact on soil composition and surface geology, contributing to a varied geological framework. The geological history of the Central Upper Peninsula of Michigan is intricate and varied, spanning billions of years and influenced by ancient geological events, glacial activities, and ongoing processes. The provided summary combines insights from the document with additional pertinent geological information.

This area, rich in geologic history and mineral resources, is of significant interest due to its potential for REEs. The geological landscape is predominantly shaped by Precambrian rocks, showcasing ancient volcanic and sedimentary processes as well as banded iron formations (BIFs) that reflect the region's history of iron ore extraction. BIFs consist of layers of iron-rich minerals and chert, serving as a crucial source of iron ore historically. The Central Upper Peninsula is underlain by Precambrian rocks, part of North America's ancient geological core, including various igneous and metamorphic types like granites, gneisses, and volcanic formations. Notably, the Marquette Trough, a significant geological feature resulting from the Penokean Orogeny during the mid-Precambrian era, is a key aspect of the region's geology. BIFs, containing iron-rich minerals interspersed with chert and other sedimentary rocks, provide clues about past oceanic conditions. These formations, extensively mined for iron ore, have contributed to the area's economic progress. Given the complex geological past of the Central Upper Peninsula and its diverse rock formations, there is potential for REEs under the right geologic circumstances. Further exploration of this potential could be worthwhile, especially considering the rising demand for REEs in the advanced technology and sustainable energy sectors. Exploration approaches might entail thorough geophysical and

geochemical surveys, building on existing knowledge of the region's geological structure to pinpoint areas with promising REEs mineralization prospects.

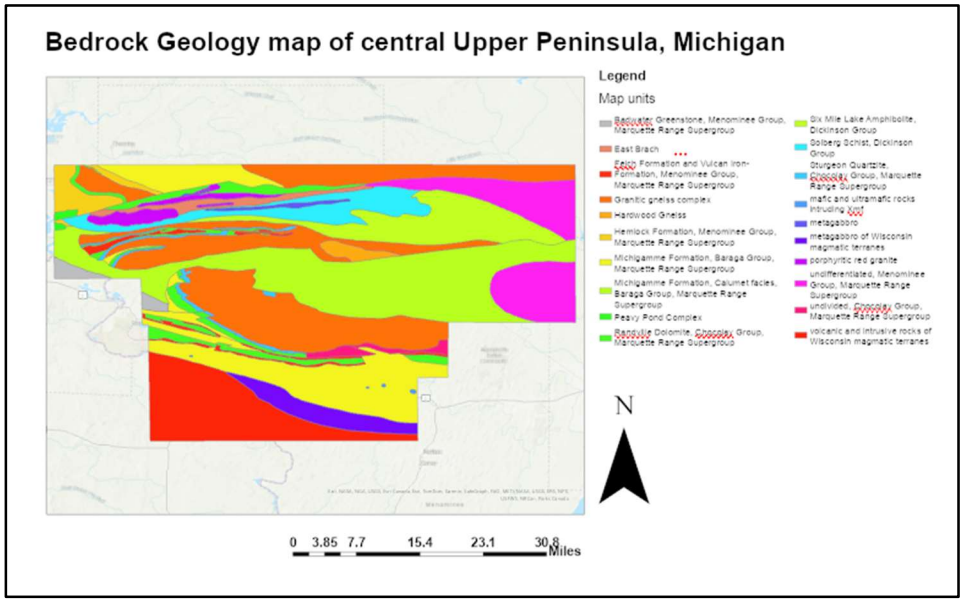

Figure 1. 2 Bedrock Geology map of the central Upper Peninsula, Michigan.

One of the historical investigations into REEs in the studied area was carried out in the Goodrich Quartzite, situated in Marquette County, Michigan, as documented in a 1987 study by B.K. Parker. The geologic map of the central upper Peninsula with different geologic units is shown in Figure 1.2. The exploration involved the analysis of ten samples from radioactive outcrops and glacial boulders in the Palmer Area, providing valuable insights into the geology and mineral potential of Michigan's central Upper Peninsula. The Palmer Area, located approximately 20 miles southwest of Marquette, exhibits Precambrian terrains containing Archean granites, lower Proterozoic metasediments, and metavolcanics. This region is characterized by the Marquette syncline and its structural complexities. The research specifically focused on the Goodrich Quartzite within this geological context, particularly examining its REEs, thorium (Th), and uranium (U) content, which displayed a strong correlation across the sampled region (Parker, 1987). Sampling primarily took place in areas with elevated radioactivity levels, targeting sections of the quartzite enriched in monazite, the primary REEs -associated mineral in the area. Chip samples weighing 0.5-1 kilogram each were collected from various locations, underscoring the limited representativeness of these samples concerning the broader outcrop areas. Neutron activation analysis was conducted on these samples to identify the presence and concentrations of REEs, Th, U, as well as elements like scandium (Sc) and gold (Au) (Parker, 1987). Examination of the quartzite's petrography indicated a composition mainly composed of angular to sub-rounded quartz with minor microcline, often altered to sericite and chlorite. Monazite, a significant inclusion, was found both within the matrix and as inclusions in quartz grains, underscoring its importance in the area's geochemistry. Geochemical assessments showed

a strong correlation among REEs in the samples, suggesting a consistent monazite composition throughout the sampled area.

The REEs patterns demonstrated enrichment in lighter REEs and distinct negative anomalies in europium (Eu), with minor anomalies in other elements (Parker, 1987). The comprehensive exploration and analysis of the Goodrich Quartzite emphasizes the substantial potential for REE extraction in the Central Upper Peninsula of Michigan. The results indicate the feasibility of resource exploitation, given the uniform mineral composition and the correlation among economically vital elements such as REEs and thorium. Parker's study lays the groundwork for further exploration and potentially the establishment of mining activities in the region, capitalizing on the unique geological characteristics of the Marquette syncline and its related formations.

3 Data and Methodology

3.1 Data

In the investigation and mapping of REEs, the combination of geochemical information and geophysical measurements presents a comprehensive approach to pinpointing abnormal areas of interest. Geochemical data play a fundamental role in this research process by providing accurate details on the concentrations and distribution patterns of heavy and light REEs throughout the surveyed area. Being primary data, they offer direct proof of the existence and levels of REEs enrichment, which are essential for assessing the economic viability of the studied region. In addition to the insights from geochemistry, gravity and magnetic surveys serve as supplementary sources of data. These geophysical techniques enable the interpretation of subsurface variations in density and magnetization that may not be readily apparent through geochemical analysis alone. Gravity data help in uncovering fluctuations in mass or density that could be linked to REEs -bearing minerals or host rocks, while magnetic data can disclose the presence of mineral phases or geological characteristics with distinctive magnetic properties that could impact the localization of REEs.

3.1.1 Geochemistry and gravity data

There were 57 geochemical data points used in this study as shown in Figure 1.3 and a total of 1536 gravity stations were obtained within the time frame of 2016 to 2019 in the central upper peninsula of Michigan and Northeastern Wisconsin as shown in igure 1.4 below.

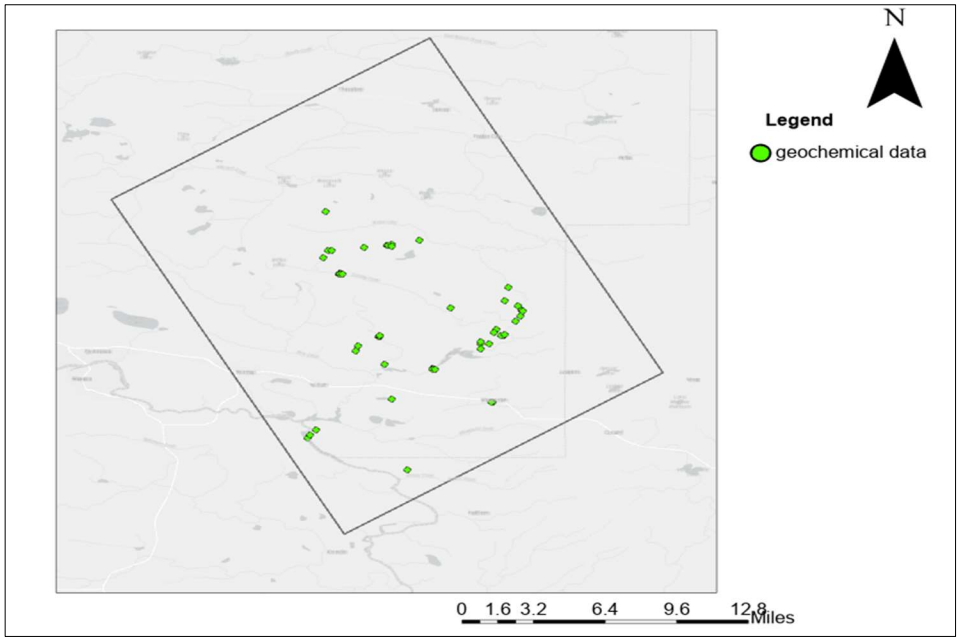

Figure 1. 3 Map of geochemistry data points in study area.

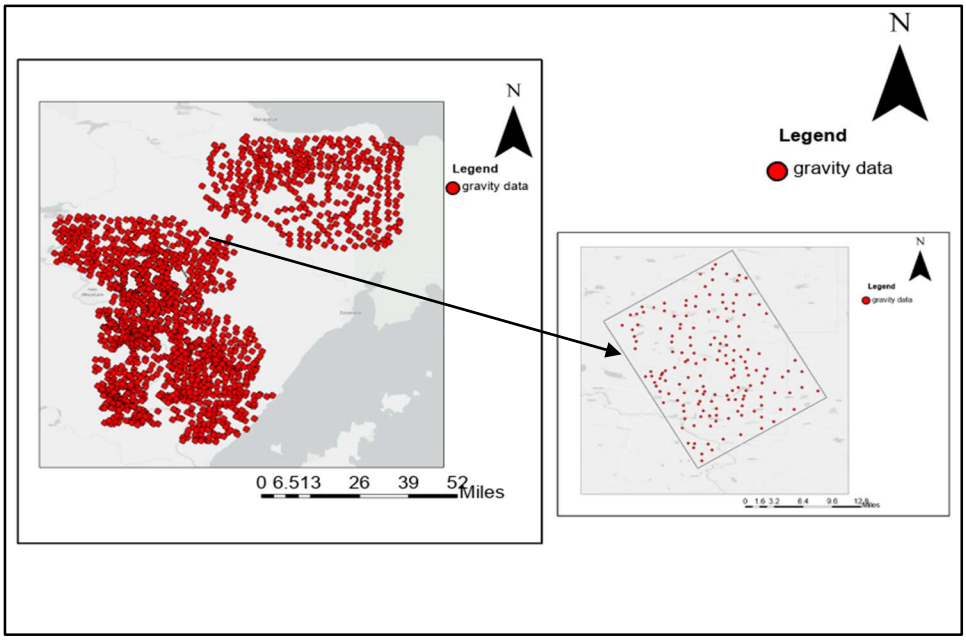

Figure 1. 4 Map of gravity data points in study area.

3.1.2 Magnetic data

According to the United States Geological Survey (2018), the airborne magnetic total-field survey was conducted in Northern Michigan to acquire high-quality geophysical data. Data collection was carried out utilizing two aircraft equipped with advanced geophysical tools, such as a cesium-vapor magnetometer for precise magnetic measurements. The survey spanned several months and covered a total of 38,474 line-kilometers of data. The flights adhered to a specific flight plan with precise line spacings and altitude requirements to optimize data quality as shown in Table 1.1. Apart from magnetic readings, the data collection process also involved synchronized recordings of positional, altimetry, and atmospheric data to facilitate comprehensive data analysis. During preprocessing, stringent quality control measures were implemented to ensure data integrity, involving the synchronization of data acquisition systems with GPS time for accurate geo-referencing of the magnetic data. Advanced onboard systems enabled real-time monitoring and adjustments, allowing for immediate responses to any data acquisition issues. Subsequently, the data underwent a re-projection process, transitioning from their initial WGS 1984 format to a standardized coordinate system known as the North American datum of 1983.

	Traverse Lines	Tie Lines	Total
Spacing	150 m	1,500 m	
Heading	North-South	East-West	
Total Line-km	34,911 km	3,563 km	**38,474 km**

Table 1. 1 Line spacing for the magnetic survey (United States Geological Survey [USGS], 2018).

The processing of magnetic data from the aerial survey involved a sequence of sophisticated corrections to refine the raw data and minimize errors. The first correction, the Partial IGRF Correction, aligned the magnetic data with the expected values of the International Geomagnetic Reference Field between the flight surface and the drape surface. Subsequently, a Diurnal Correction was applied to address daily fluctuations in the Earth's magnetic field, separating geological anomalies from these variations. Intersection Leveling ensured consistency across intersecting flight lines through statistical analysis and adjustment. Furthermore, Taylor Correction compensated for altitude deviations from the planned flight path to maintain data accuracy over diverse terrain. Lastly, Micro-Leveling was utilized to fine-tune the data by eliminating small-scale variations and enhancing the smoothness of the magnetic data presentation. These corrections played a crucial role in minimizing the impact of environmental, instrumental, and operational factors that could potentially distort the magnetic data. The processed data underwent a final round of quality controls, including gridding and detailed analysis, to validate the accuracy of the magnetic data in representing subsurface geological characteristics (United States Geological Survey [USGS], 2018). The total magnetic field data is shown below in Figure 1.5 and the integration of the primary data, the geochemical and the secondary data sources, gravity, and magnetic data, is also shown in Figure 1.6.

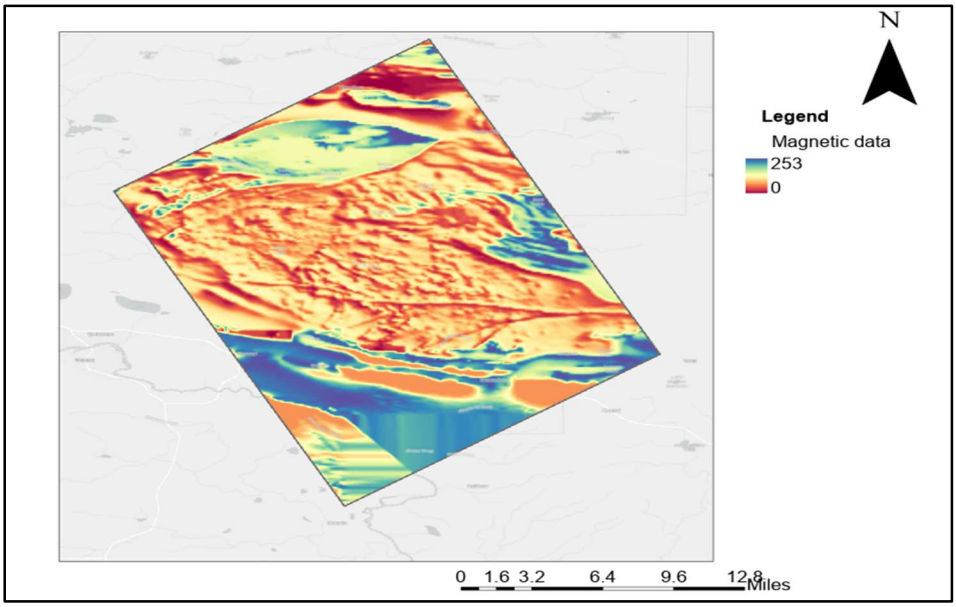

Figure 1. 5 Map of magnetic field data in study area.

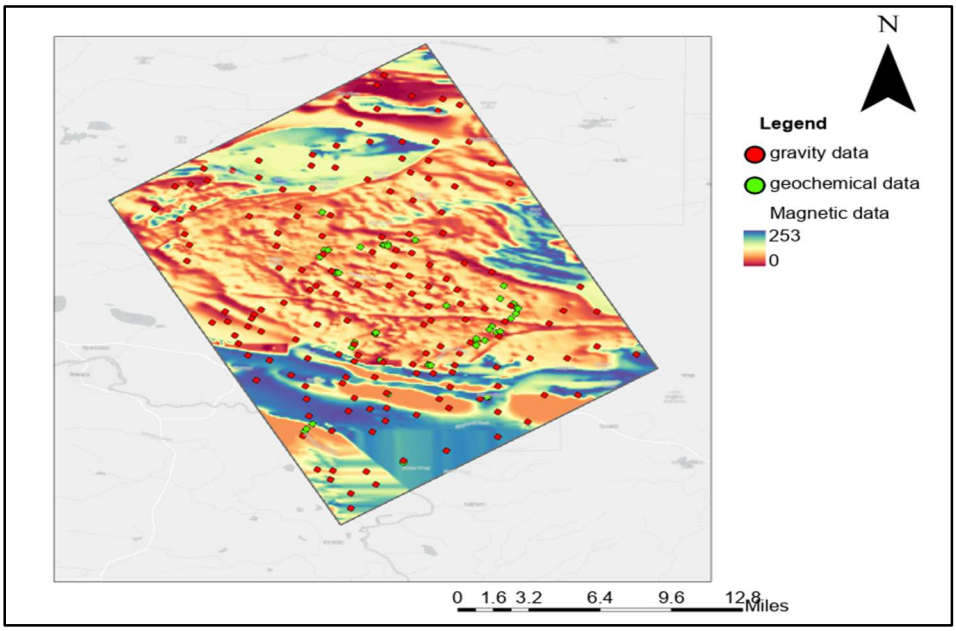

Figure 1. 6 Map of combined data in study area.

3.1.3 Data pre-processing and resampling

The geochemical and gravity point data and the magnetic raster data were loaded, and pre-processing was carried out. All data were geo-referenced. All null values from the raster data. The nearest neighbor resampling technique was utilized for adjusting the cell

sizes and spatial resolution of the raster files and it is an efficient approach. With nearest neighbor resampling, every pixel in the resulting raster is assigned the value of the nearest pixel from the initial raster, determined by the geometric center of each output pixel. The data analysis further checks for missing values, conversion of raster data to points and vice versa, checking the distribution pattern which shows some level of correlation between the datasets. The mosaic to new raster tool was eventually used to merge the magnetic raster data.

3.2 Methodology

At the heart of the methodology lies the application of spatial continuity modeling to analyze the spatial correlations of LREEs and HREEs concentrations in geochemical data. This is integrated with gravity and magnetic datasets through coring, a multivariate geostatistical technique facilitating the integration of secondary data sources with primary geochemical data. This integration offers a more detailed prediction of HREEs and LREEs distribution by leveraging spatial correlations across different data types. Subsequently, fractal analysis is used to examine the complexity and scaling behavior of the geochemical, gravity, and magnetic datasets, unveiling anomaly distribution patterns that may highlight zones of higher REEs enrichment.

The results phase combines findings from geochemical data with gravity and magnetic anomalies to pinpoint potential hotspots for HREEs and LREEs mineralization. The conclusion synthesizes insights gained from this integrated approach, underscoring the improved predictive power and accuracy that contributes to anomaly mapping and exploration. By incorporating geophysical datasets, the methodology not only enhances the geochemical perspective but also offers a comprehensive three-dimensional understanding of the geological environment, advancing the exploration process towards new frontiers of efficiency and effectiveness.

3.3 Spatial continuity modeling

In this study, the methodology relies heavily on spatial continuity modeling, which is fundamental for accurately characterizing and predicting the HREEs and LREEs anomalies. The initial step involves creating variograms, essential tools for evaluating the level and extent of spatial correlation in our primary geochemical and secondary data sources. To account for anisotropic conditions, where variability depends on direction, our analysis includes variogram maps to depict semi-variance in various directions, offering a holistic perspective of the spatial arrangement. This analysis uncovers directional relationships and inconsistencies within the data sets, crucial for grasping the intricate geological factors influencing the distribution of REEs. The spatial models based on variograms are then fine-tuned and verified using cross-validation techniques to ensure their reliability. Once we establish dependable models of spatial continuity, we implement cokriging, a multivariate geostatistical approach.

3.4 Co-kriging

Co-kriging is a complex geostatistical method utilized to estimate the values of a main variable at locations where data is lacking by incorporating both the main variable and one or more secondary variables that exhibit a correlation with it. This technique proves advantageous when there is limited data available for the main variable but an abundance of data for the secondary variable(s), thus leading to an enhancement in the accuracy of estimation. Various forms of co-kriging, such as simple, ordinary, and universal co-kriging, are tailored to suit the specific characteristics of the data and the inherent spatial patterns. The core idea behind co-kriging is that the supplementary information from the co-variable can improve the estimation (prediction) of the target variable by exploiting the cross-correlation between the variables. This process assumes that the regionalized variables have a multivariate spatial cross-correlation as well as a univariate spatial autocorrelation.

The co-kriging general equation can be written as:

$$z_0^* = \sum_{i=1}^{n} \lambda_i z_i + \sum_{j=1}^{n} \beta_{1j} y_{1j} + \sum_{k=1}^{n} \beta_{2k} y_{2k}$$

Where:

Z_0^* (s_0) is the estimated value at the target location.

λ_i are the weights for the primary variable at known locations z_i.

$\beta 1j$ are the weights for the first secondary variable at known locations $y1j$.

$\beta 2k$ are the weights for the second secondary variable at known locations $y2k$.

n is the number of known data points used in the estimation for each variable.

The weights λ and μ are determined such that the estimation error variance is minimized, subject to the condition that the estimator is unbiased. This is typically done by solving a system of linear equations derived from the variogram or covariance functions of the primary and secondary data. This system includes direct variograms for each variable and cross-variograms (or covariograms) between each pair of variables. Co-kriging was employed in this study, and this involves utilizing the spatial correlation between dense gravity and magnetic data and sparse geochemical measurements to calculate geochemical values at unsampled locations. This approach capitalizes on the extensive coverage of gravity and magnetic surveys to enhance the interpolation of geochemical parameters, under the assumption that these data categories exhibit spatial correlation. The process includes constructing variograms and cross-variograms, fitting a suitable model to these data, and then using the model to estimate the primary variable across the area of interest.

In this study, a simple co-kriging approach was utilized. The main variable of interest is Z_1, and both autocorrelation for Z_1 and cross-correlations between Z_1 and all other variable types are used to make better predictions. LREEs and HREEs are the main variables while the gravity and magnetic data are the secondary variables. Each $Zi(s)$ variable exhibits a distinctive autocorrelation [pattern] outlined by its variogram or semivariogram, which characterizes the spatial correlation of $Zi(s)$ with itself at varying lags. Additionally, there exist interrelationships between the primary and secondary variables, captured by cross-variograms or cross-semivariograms, which quantify the way one variable changes in relation to variations in another across different lags. Mathematically, the equation would be as shown below:

$$z^*_{\mathrm{LREE}}(\mathrm{s0}) = \sum_{i=1}^{n} \lambda_i z_{LREE}(\mathrm{si}) + \sum_{j=1}^{m} \lambda_j z_{HREE}(\mathrm{sj}) + \sum_{k=1}^{o} \lambda_k z_{CBA}(\mathrm{sk}) + \sum_{l=1}^{p} \lambda_l z_{MRESLVLD}(\mathrm{sl})$$

where

z^*_{LREE} (s_0) is the predicted value of LREEs at the unsampled location s_0.

λ_i are the weights assigned to the observed values of LREEs at sampled locations s_i based on their spatial correlation with s_0.

z_{LREE} (s_i) are the observed values of LREEs at location s_i

λ_j, λ_k, λ_l are the weights for the observed values of the secondary variables HREEs, CBA, and MRESLVLD, respectively.

z_{HREE} (s_j), z_{CBA} (s_k), and z_{MRESLVLD} (s_l) are the observed values of the secondary variables of HREEs, CBA, and MRESLVLD at location s_j, s_k, and s_l, respectively.

n, m, o, and p are the numbers of observed values for LREEs, HREEs, CBA, and MRESLVLD that are being considered in the estimation process, respectively.

3.5 Concentration-area (C-A) fractal model analysis

The C-A fractal model is a quantitative technique commonly utilized in the fields of geochemistry and mineral exploration for the purpose of examining and interpreting spatial distributions of geochemical element concentrations within a specified area. The foundation of the C-A fractal model lies in the recognition that mineralization processes frequently give rise to patterns of element concentrations that demonstrate fractal characteristics. These patterns can be scrutinized to differentiate between the baseline (typical levels found in the earth's crust) and anomalies (elevated concentrations suggestive of mineral deposits). Fractal models were used to compute the thresholds of HREEs and LREEs. The log plots were generated and used to establish the thresholds.

The concentration maps showing the concentration of HREEs and LREEs were created by plotting their concentration values (C) against the area of cells (A). In addition, the log-log plots of C-A were generated for HREEs and LREEs concentration to calculate the specific thresholds. Finally, a classification map was generated to identify geochemical anomalies of HREEs and LREEs.

In this study, the calculation of the minimum 'min_est' and maximum 'max_est' estimated values for the predicted variable 'var1.pred' from the raster dataframe 'raster_df' is conducted. A sequence ranging from the minimum to the maximum estimated value with an interval of 0.01 is established for the purpose of thresholding the predicted values. Subsequently, within a loop, each threshold in 'grd_inter' is examined by the script to determine the predicted values surpassing the current threshold, counting them, and storing the count as 'num_pix'. This tally is then recorded alongside the threshold value in a matrix 'grade'. Lastly, a log-log plot illustrating the thresholds against their corresponding counts is generated. The identification of thresholds was carried out using the segmented linear regression (SLR) approach, employing a maximum of 20 breakpoints. The code systematically fits segmented linear regression models with an increasing number of breakpoints to the log-transformed data, halting when no significant enhancement in model fit is observed, and consequently determining the most suitable number of breakpoints. A linear model is applied to the data, and the segmented () function is utilized to fit a segmented linear model, potentially pinpointing a breakpoint where the linear relationship shifts. Following the loop execution, the value of 'i' at which the loop terminated indicates the optimal number of breakpoints considered based on the enhancement of R-squared. A test involving various interval values revealed that 0.01 yielded the best outcomes in this study, resulting in the generation of 11 breakpoints which is about 10 thresholds. Furthermore, a plot of the calculated data and fitted data was generated and various classification maps were also generated.

4 Results

4.1 Spatial continuity modeling

4.1.1 Light rare earth elements (LREEs)

The results of the analysis on the concentration of LREEs are depicted through an empirical semi-variogram that shows an initial rise in semivariance values, starting from close to zero and stabilizing after reaching a distance of 0.06 units as shown in Figure 1.7 and this pattern indicates the presence of spatial autocorrelation in LREEs concentrations within this specific range. Cases of anisotropy were also investigated to check if the data exhibit some form of directional variability. Some forms of weak anisotropy were detected in the data. For example, in Figure 1.8, a plot of 4 directions (0, 45, 90, 145) was plotted and we see a case of weak anisotropy in the 0-degree direction especially with increasing distances where semivariance values are notably elevated. This indicates a more pronounced spatial variability in that specific direction. Conversely, at shorter distances, semivariance values for angles 45, 90, and 145 are closely clustered, demonstrating significant overlap and suggesting a more isotropic behavior along these directions as seen in Figure 1.9 and while the differentiation between semivariance values for various directions is less pronounced, the observed variation, especially for direction 0, implies directional disparities in the spatial data, with the most prominent anisotropy observed over long distances.

Through cross-validation, the comparison between predicted and actual values reveals an average prediction error of 4.599, with residuals ranging from -144.317 to 502.632. Figure 1.10 Despite this wide range, the central tendency of the residuals indicates no bias in the model's predictive accuracy. These empirical results underscore the model's capability to estimate LREEs concentrations reliably, while also pointing out areas for enhancement, especially in predicting higher concentration levels where notable discrepancies were observed.

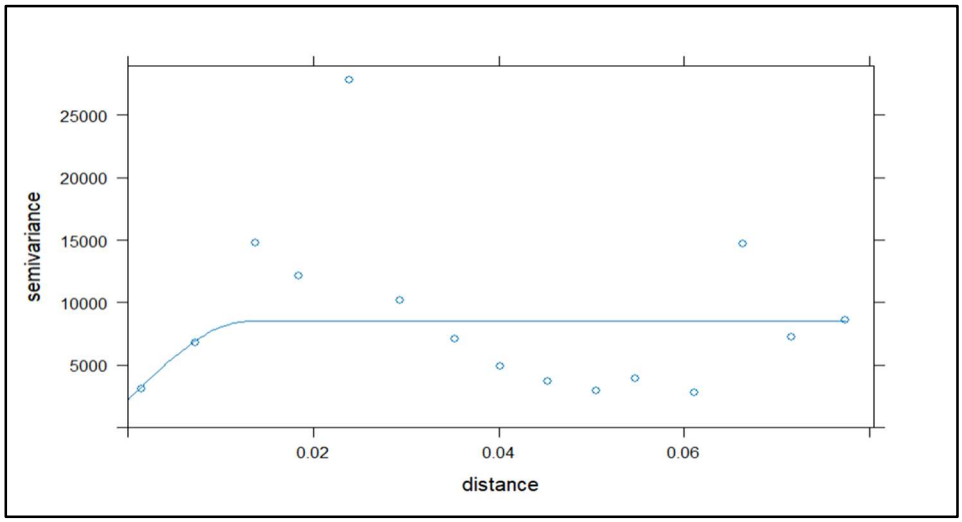

Figure 1. 7 Experimental semi-variogram of LREEs.

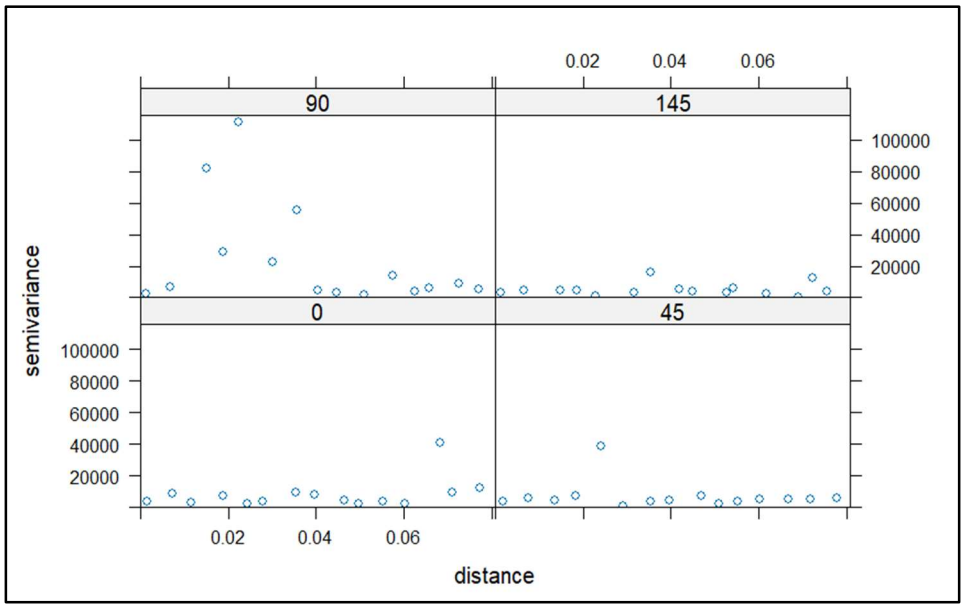

Figure 1. 8 Directional variogram of LREEs.

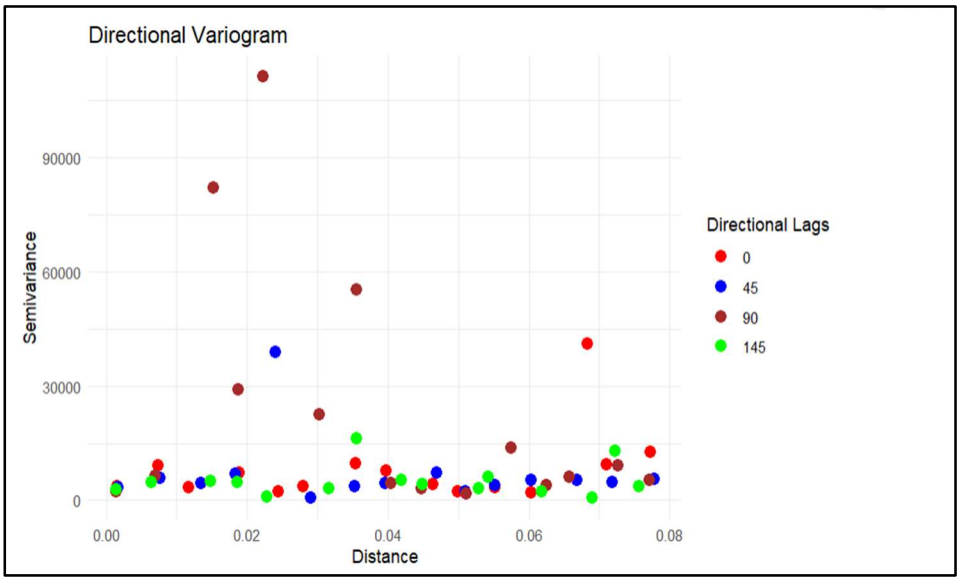

Figure 1. 9 Directional variogram plot of LREEs.

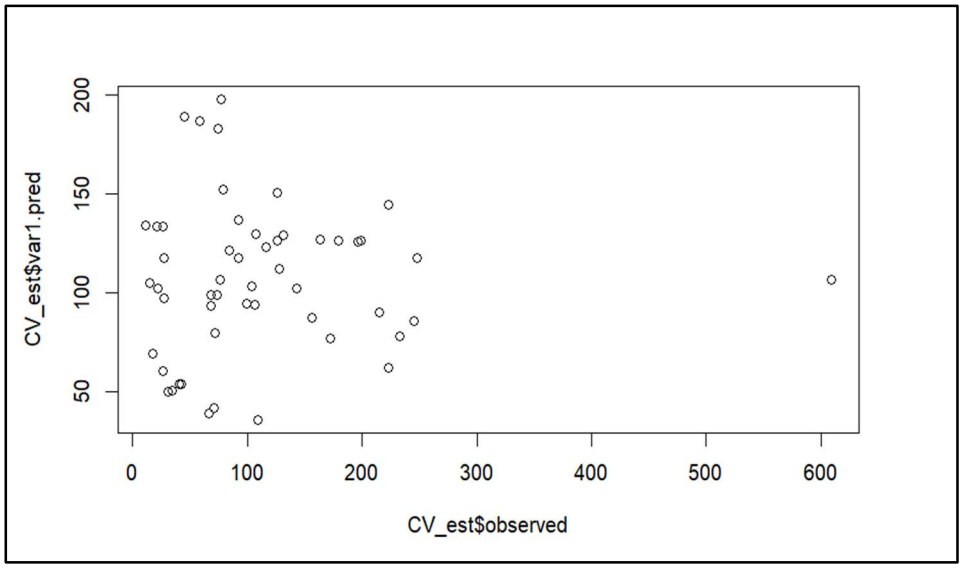

Figure 1. 10 Coefficient of variation plot of LREEs.

residual	
Min.	-144.317
Ist Qu.	-46.499
Median	-12.740
Mean	4.599
3rd Qu.	43.464
Max.	502.632

Table 1. 2 Coefficient of variation statistics of LREEs.

The LREEs interpolated map in Figure 1.11 shows the spatial variation of the concentration of LREEs across the study area. Regions exhibiting the most elevated levels of Light Rare Earth Elements (LREEs) are depicted by more intense hues, notably situated in the lower right section of the visual representation (signifying the uppermost range of 343.162 - 461.95). Conversely, regions with the least concentrations are illustrated in paler shades, for instance, in the upper left corner (indicating the lowermost range of 12.317 - 52.683).

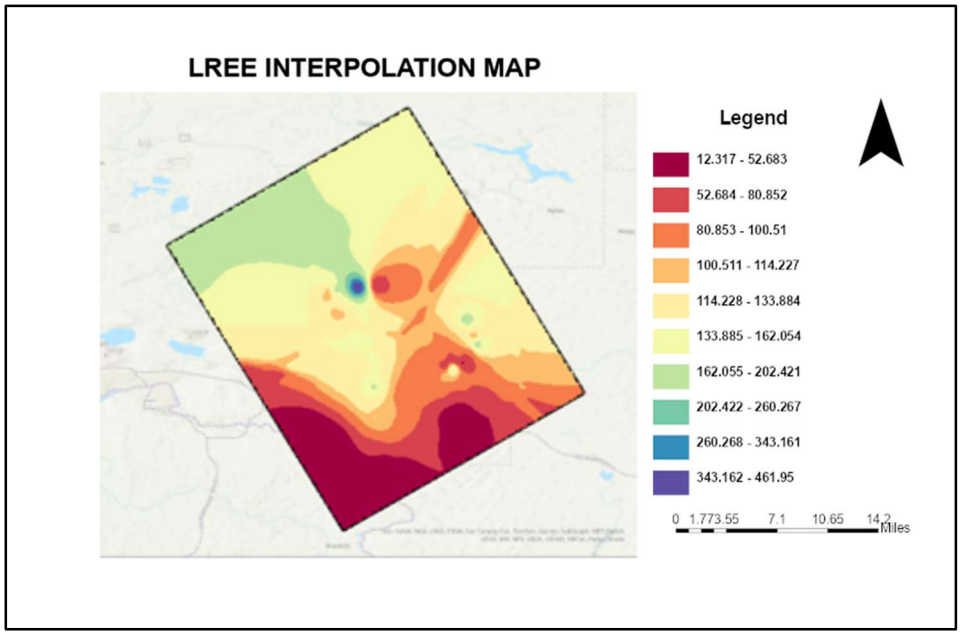

Figure 1. 11 Interpolated map of LREEs.

4.1.2 Heavy rare earth elements (HREEs)

The results of the analysis of HREEs show a semivariance pattern that bears some semblance with the LREEs. Figure 1.12 shows the empirical semivariogram plot with an initial sharp increase, indicating a strong spatial relationship at shorter distances. This rapid rise implies that concentrations of HREEs vary more noticeably when samples are taken in proximity, a common trait in mineral deposits where areas of high concentration can be found. As the distance between samples increases, the semivariance values start to level off, indicating a decrease in the spatial correlation among samples. This stabilization in the variogram, referred to as the sill, seems to occur at approximately 0.06 units of distance, beyond which the variation between sample points does not notably increase. This indicates a maximum limit to the spatial impact, after which samples do not exhibit a strong spatial connection. The trend seen in the experimental variogram remains consistent across directional variograms examined, with directional variograms at 0, 45, 90, and 135 degrees all displaying similar behavioral patterns. This isotropy demonstrates that the spatial correlation of HREEs concentrations is not greatly influenced by the measurement direction. The scatter plot from cross-validation, which compares estimated and observed values, lacks a clear trend, suggesting the possibility for enhancing the model's predictive accuracy. Residual analysis indicates a consistent average close to zero, indicating a model without bias.

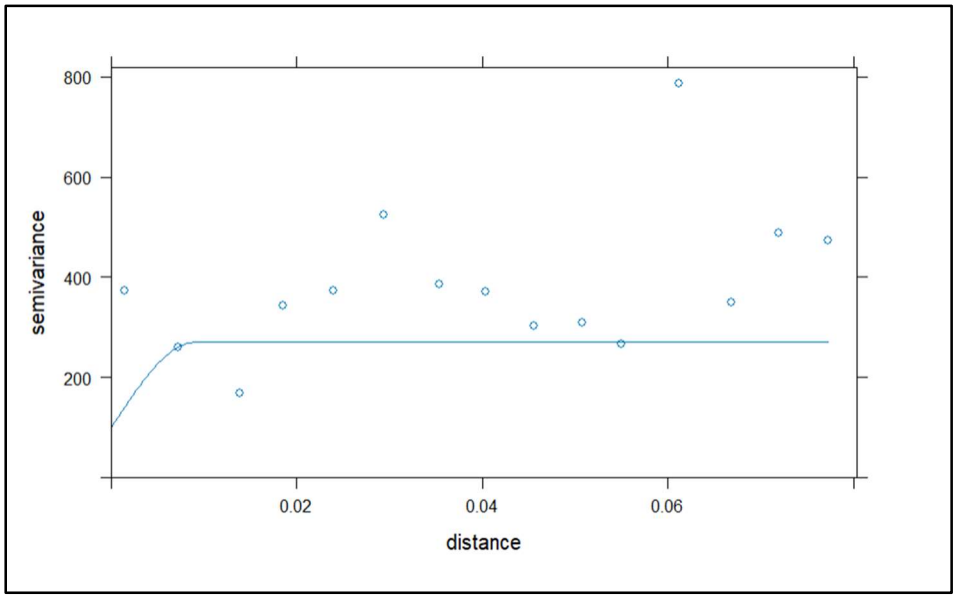

Figure 1. 12 Experimental semi-variogram of HREEs.

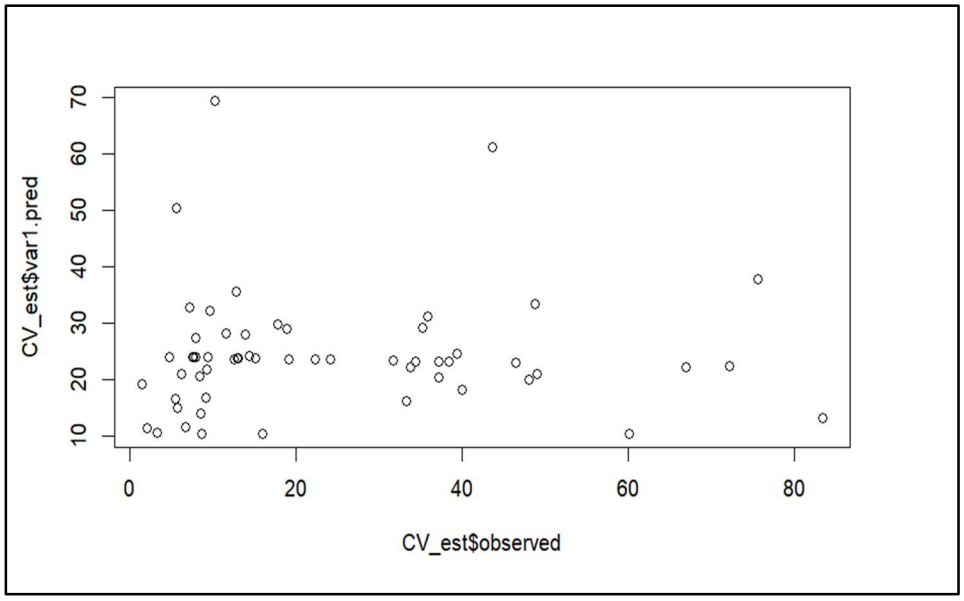

Figure 1. 13 Coefficient of variation plot of HREEs.

In conclusion, the HREEs does exhibit spatial continuity within a specific range, beyond which sample values are not strongly correlated. This insight can inform further geochemical analysis and exploration endeavors, where refining sampling strategies to focus within distances showing the strongest spatial correlations can enhance resource estimation. This interpolation map displays a spatial analysis of concentration levels of HREEs in the study area. The legend's color gradient corresponds to the values of HREEs concentration with the dark blue sections depicted on the map signifying the areas with the most significant accumulations of HREEs, implying promising locations for

additional examination or investigation. In contrast, the paler, yellow areas denote lower concentrations of HREEs. This map serves as a crucial instrument for pinpointing geological areas of interest pertaining to the distribution of HREEs.

residual	
Min.	-59.1120
Ist Qu.	-14.4523
Median	-7.6776
Mean	-0.3893
3rd Qu.	14.0353
Max.	70.1633

Table 1. 3 Coefficient of variation statistics of HREEs.

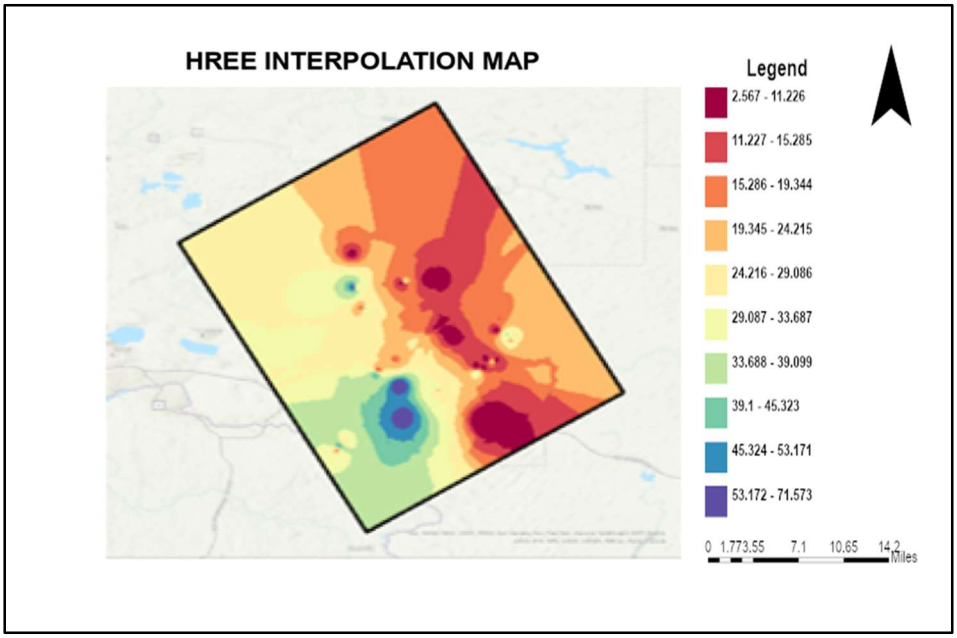

Figure 1. 14 Interpolated map of HREEs.

4.1.3 Gravity data

The semi-variogram plot of the gravity data indicates a consistent lack of an initial variance jump as seen in Figure 1.15, which suggests the absence of a nugget effect and supports the reliability of measurements. The gradual increase in semi-variance as distance grows demonstrates a common spatial autocorrelation pattern, indicating that nearby locations exhibit similar gravity values.

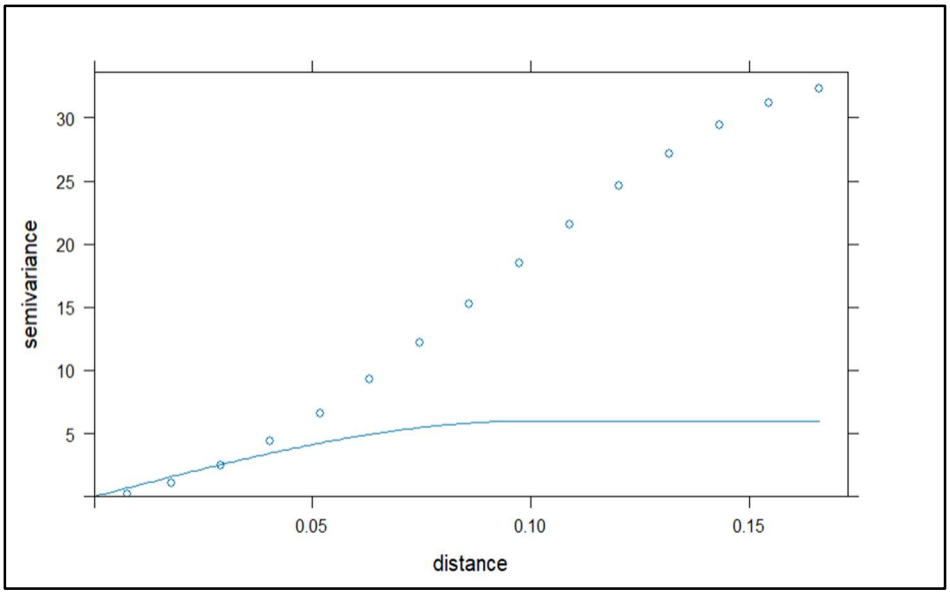

Figure 1. 15 Experimental semi-variogram of gravity data.

4.1.4 Magnetic data

The magnetic data variogram plot shown in Figure 1.16 illustrates a positive relationship between data variability and distance. It initiates with a nonzero "nugget," indicating unexplained variability at very short distances or potential measurement errors. As semivariance values increase, they reach a "sill," which signifies the point where data correlation ceases. The distance at which this plateau occurs, referred to as the "range," determines the spatial correlation extent. Beyond this range, data points no longer impact each other's values significantly, suggesting spatial lack of correlation at greater distances. The curve's shape resembles that of a spherical model.

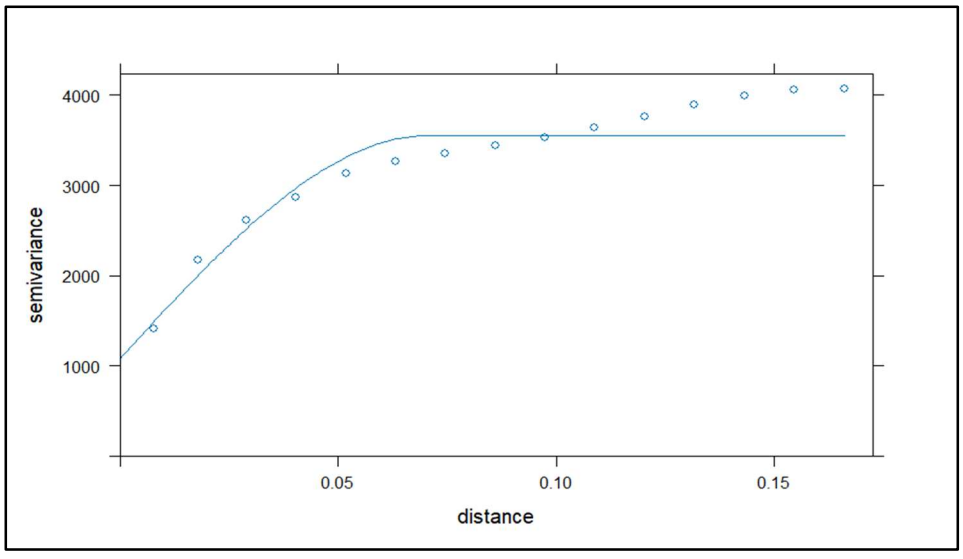

Figure 1. 16 Experimental semi-variogram of magnetic data.

4.2 Cross variograms

Figure 1.17 shows a cross-variogram which demonstrates the spatial connection between LREEs and HREEs, showing a positive correlation at shorter distances that decreases as distance increases. This indicates a level of spatial interdependence between the two elements in the research area. In Figure 1.18, the cross-variogram plot shows the association between LREEs and gravity data, uncovering a weaker correlation in comparison to the LREEs and HREEs relationship. The variogram exhibits a less prominent pattern, implying a reduced spatial relationship between LREEs distribution and gravity anomalies.

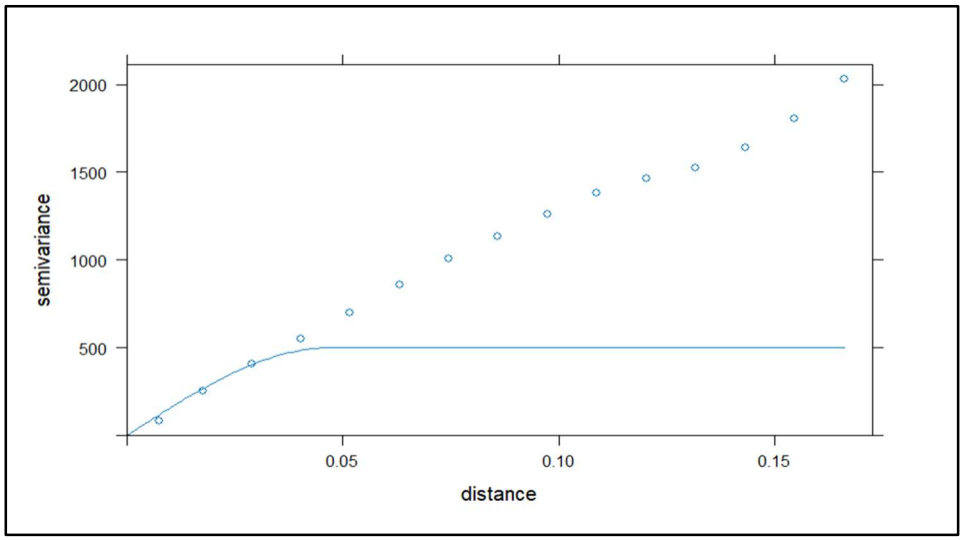

Figure 1. 17 Cross variogram of LREEs and HREEs.

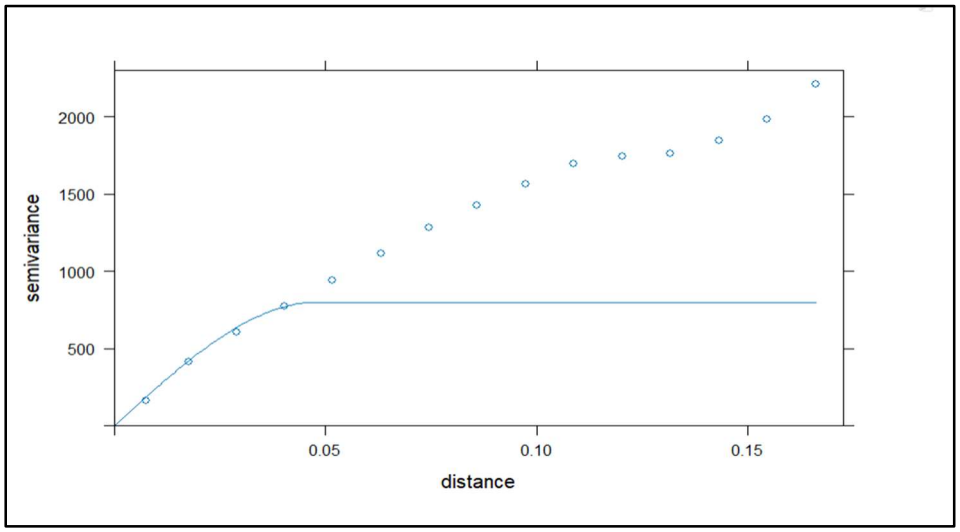

Figure 1. 18 Cross variogram of LREEs and Gravity data.

4.3 Cross validation

In the co-kriging semi-variogram model for the LREEs shown below, the blue curve, which represents the measured values fits with the predicted values reasonably well as shown in Figure 1.19. The minimal mean error suggests the absence of a notable systematic bias. The distribution plot of residuals indicates potential variability not accounted for by the model, potentially stemming from outliers or unrepresented spatial patterns.

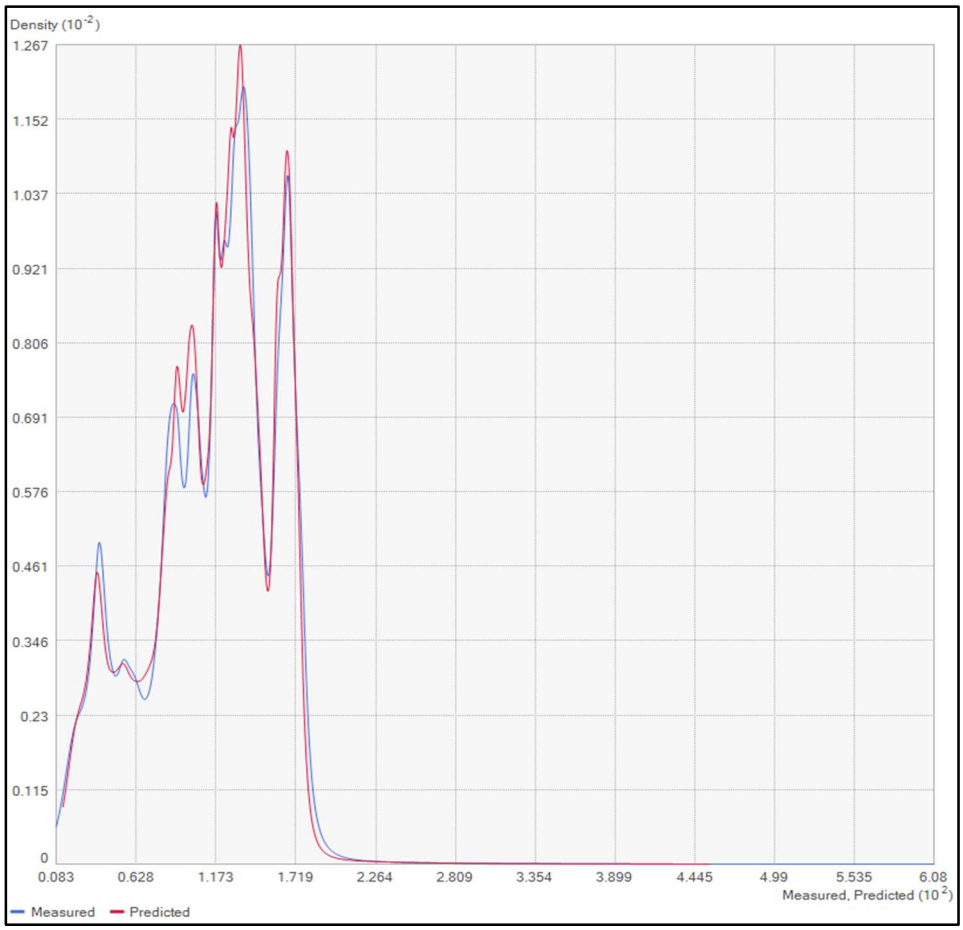

Figure 1. 19 Co-kriging measured and predicted values of LREEs.

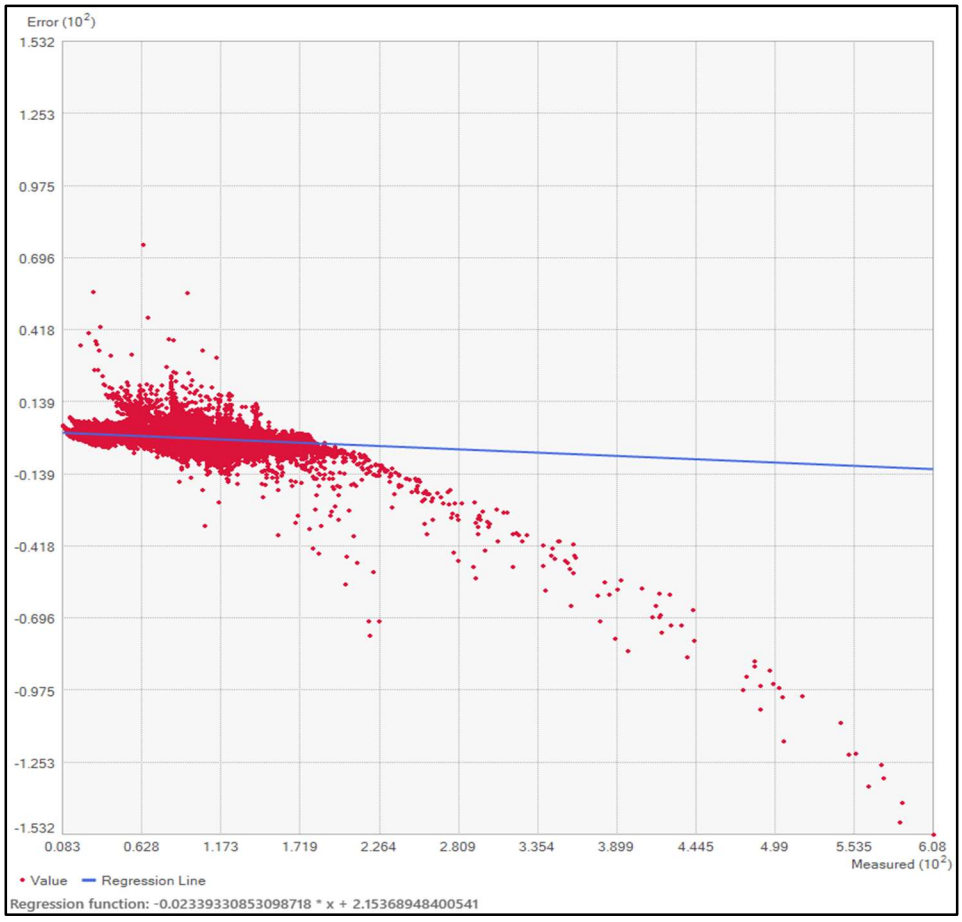

Figure 1. 20 Co-kriging error plot of LREEs.

The error plot for the LREEs, gravity, and magnetic data cross-validation shown below as Figure 1.20 reveals a significant dispersion of residuals compared to observed values, indicating variability in the predictive capability of the model. The concentration of data points around the zero line suggests that numerous predictions closely match actual values, yet there is noticeable dispersion, indicating instances of both over and underestimation. The cross-validation results of the cokriging model reveal a minor overestimation bias and a mean standardized error close to zero, indicating an accurate distribution of errors. The model exhibits a strong fit, with the standardized RMS being nearly one, and an RMS error of around 5.07. This suggests a reasonably good fit for the model, especially given the intricacies of geological data, showcasing dependable predictions when incorporating LREEs alongside gravity and magnetic data.

Summary statistics	
Mean	-0.6515
RMS	5.0745
Mean Standardized	-0.0390
RMS Standardized	0.2004
Average Standard Error	19.6152

Table 1. 4 Cross-validation residual statistics of LREEs.

The result of the cross validation of the co-kriging model involving HREEs and the secondary variables are also shown below in Figures 1.21 and 1.22. The cross-validation results for the co-kriging of HREE data with gravity and magnetic data illustrate the model's predictive performance. The density plot indicates a notable correspondence between the measured and predicted values, with a trend that shows fluctuation patterns aligning in most regions. This suggests that the model can capture the variations in HREE concentrations to some extent. The error plot displays a widespread distribution of errors around zero, which is indicative of a lack of systematic bias in the predictions. However, the presence of outliers, especially those with higher errors, points to certain predictions that significantly differ from the observed values. The regression line across the error plot, relatively flat, also supports the notion of a minimal bias across the prediction range.

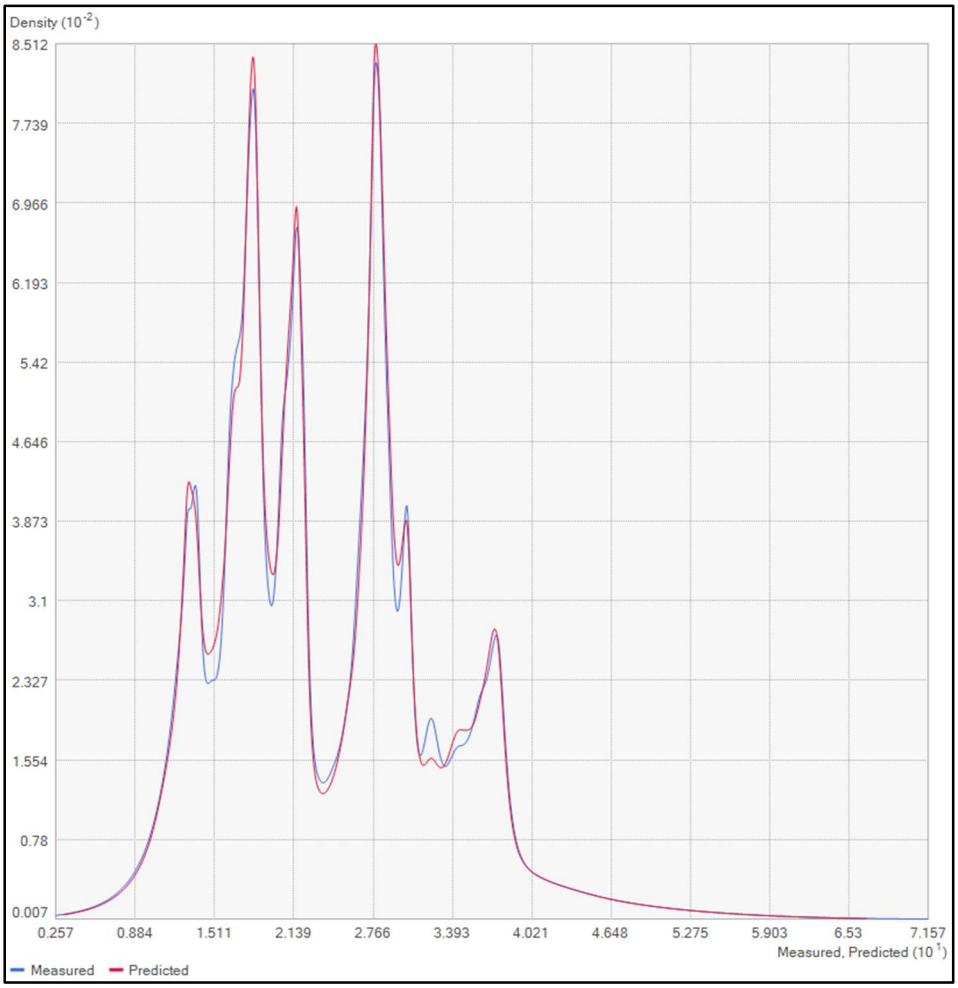

Figure 1. 21 Co-kriging measured and predicted values of HREEs.

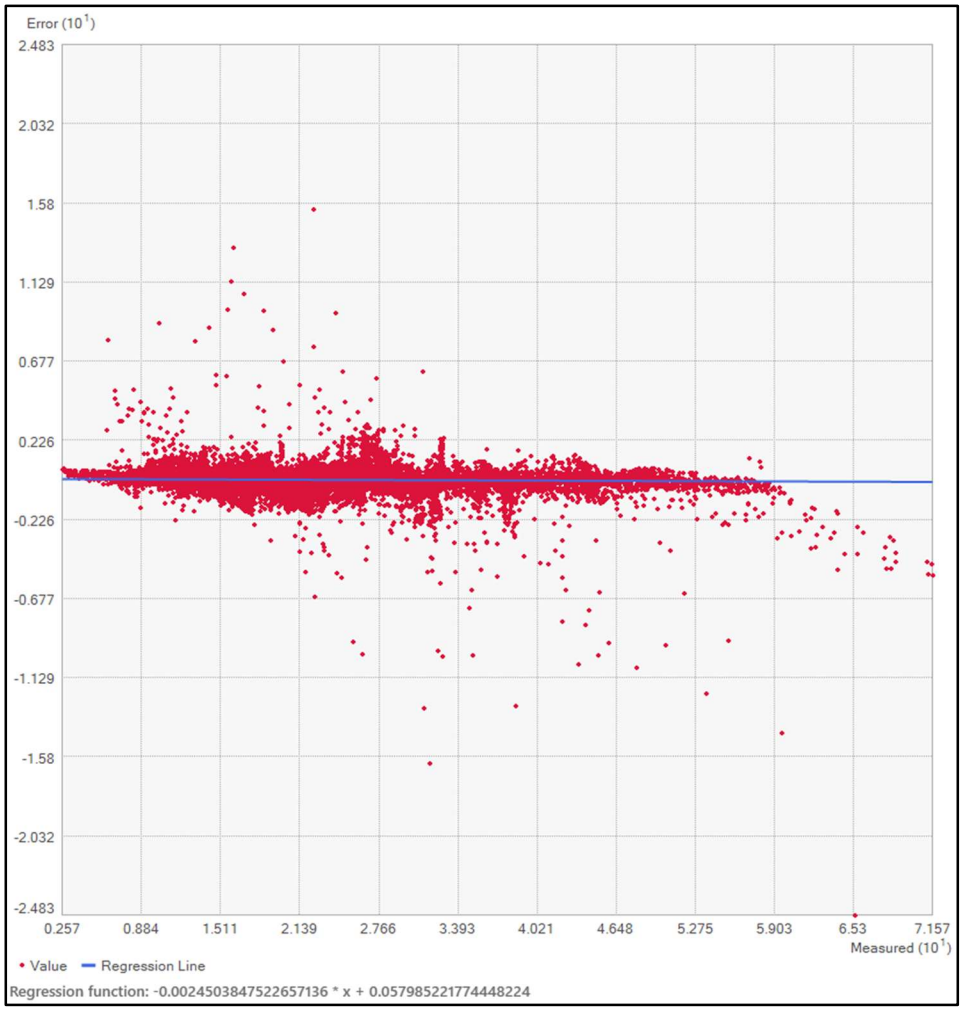

Figure 1. 22 Co-kriging error plot of HREEs.

Summary statistics	
Mean	-0.0083
RMS	0.5834
Mean Standardized	-0.0086
RMS Standardized	2.1195
Average Standard Error	0.2938

Table 1. 5 Cross-validation residual statistics of HREEs.

4.4 Fractal modeling

The concentration values plotted against area is depicted by the red line on this graph. The green lines are the identified breakpoints that segregate distinct populations within the dataset. The (C-A) log-log plots for LREEs and HREEs are both shown below as Figure 1.23 and 1.24 and the LREEs plot is characterized by a trend in which the initial log-concentration values show a high magnitude (e.g., between 2 to 4 on the logarithmic scale), resulting in a sharp rise on the left side of the graph. This pattern indicates an accumulation of LREEs in specific areas that significantly differ from the standard crustal abundance, identifying them as geochemical anomalies. As the log scale distance increases (approaching 0 or negative values), the semivariance values stabilize, implying that most locations exhibit lower LREEs concentrations, aligning with the typical background levels found in the Earth's crust.

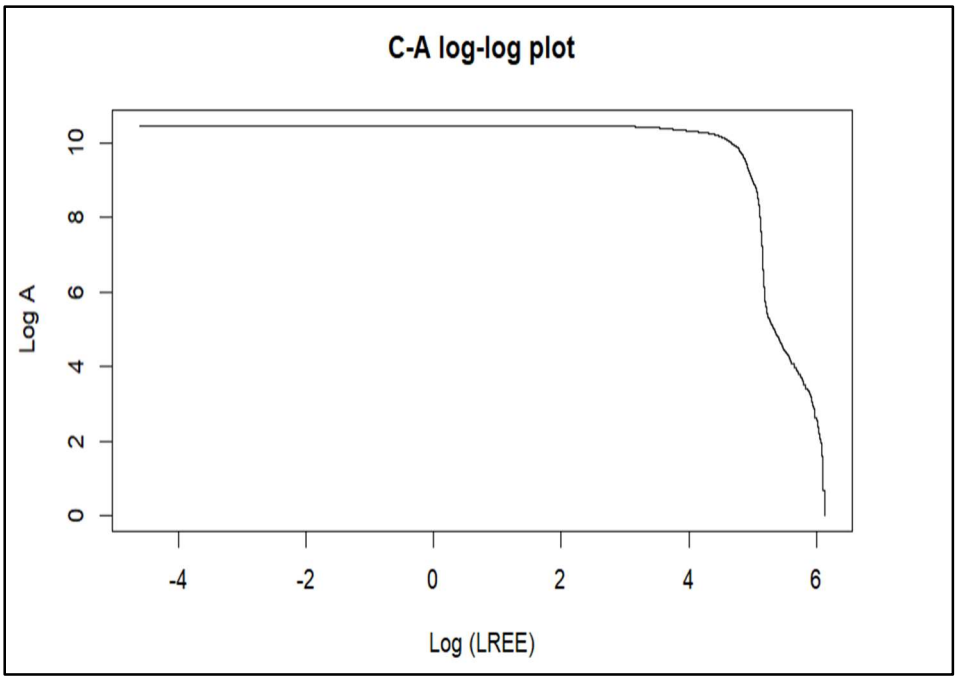

Figure 1. 23 C-A log-log plot for LREEs.

In the context of the HREE plot, if a similar trend to that observed in the LREEs is identified, characterized by elevated initial log-concentration values (potentially ranging from 1 to 3 on the logarithmic scale), this signifies notable enrichment of HREEs regions. The point of inflection, where the plot starts to level off (which may occur at a log-distance value of approximately 0 to 1), marks the boundary between abnormal concentrations and the broader, lower baseline levels. A gentler initial incline in comparison to the LREE could indicate a lesser concentration of HREEs or a distinct spatial distribution influenced by geological factors. In both scenarios, the inflection point or 'elbow' plays a critical role by indicating a shift from high-grade ore zones to more scattered, lower-grade areas, with the steepness of the curve offering insights into the extent and scope of the anomalies. The specific thresholds at which the curve alters

provide pivotal benchmarks for defining the demarcation between abnormal and background concentrations within the surveyed area.

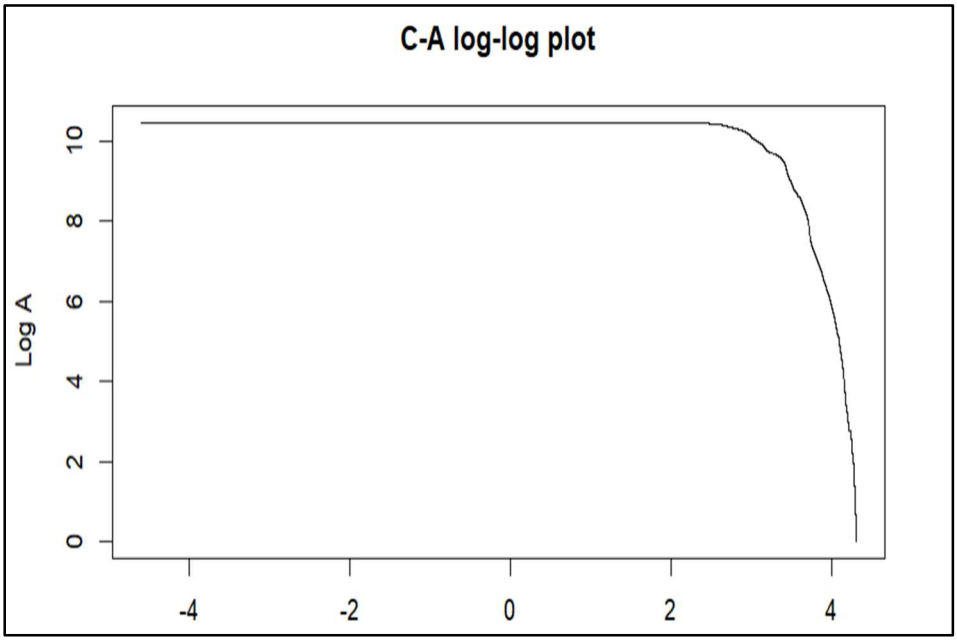

Figure 1. 24 C-A log-log plot for HREEs.

The distribution of LREEs displays a sharp initial incline, indicating elevated concentrations in specific areas, suggesting notable geochemical irregularities related to LREEs. After this steep rise, the graph plateaus, illustrating a swift decline in LREEs levels across most sites, in accordance with a typical distribution pattern observed in the Earth's crust. The depiction of HREEs in the second graph closely resembles the LREEs trend, featuring a steep initial segment that highlights the presence of high concentrations of HREEs in some regions. This segment then transitions into a flat phase, signifying a decrease in anomalies and a broad reduction in abundance at higher locations. Both illustrations imply that only a limited number of sites exhibit elevated levels of LREEs and HREEs, making them potentially valuable for mineral exploration, while most locations show significantly lower concentrations. The geochemical QQ plots shown as Figures 1.25 and 1.26 validate a consistent distribution pattern for both LREEs and HREEs, characterized by notable irregularities followed by a multitude of sites with background levels of rare earth elements.

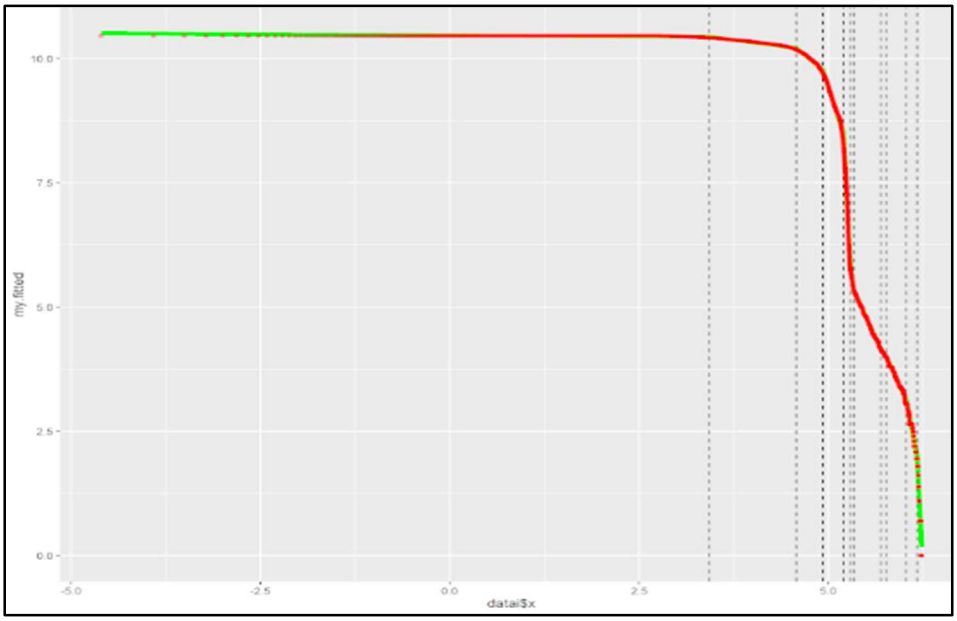

Figure 1. 25 QQ plot for LREEs.

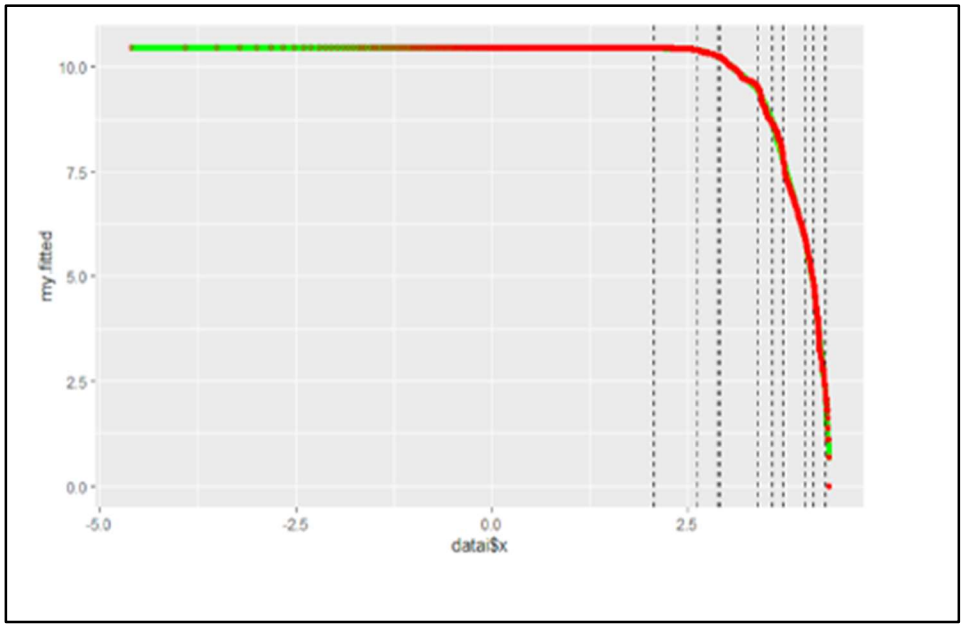

Figure 1. 26 QQ plot for HREEs.

The steepness of the slope on the right side implies a substantial alteration in area with minor concentration variations, a common sign of high anomaly concentrations in a limited area – corresponding to the red regions on the classification map. Taken collectively, the QQ and C-A plots suggest the presence of at least one notable geochemical anomaly in the examined region that may necessitate further investigation. This anomaly is characterized by a high abundance of LREEs, as indicated by the class 10 categorization on the map and

the corresponding threshold on the C-A plot. The existence of such a notable anomaly could hint at underlying mineralogical processes that have enriched this region with LREEs. There are 10 thresholds identified for the LREEs based on (C-A) log-log plots of the combined data

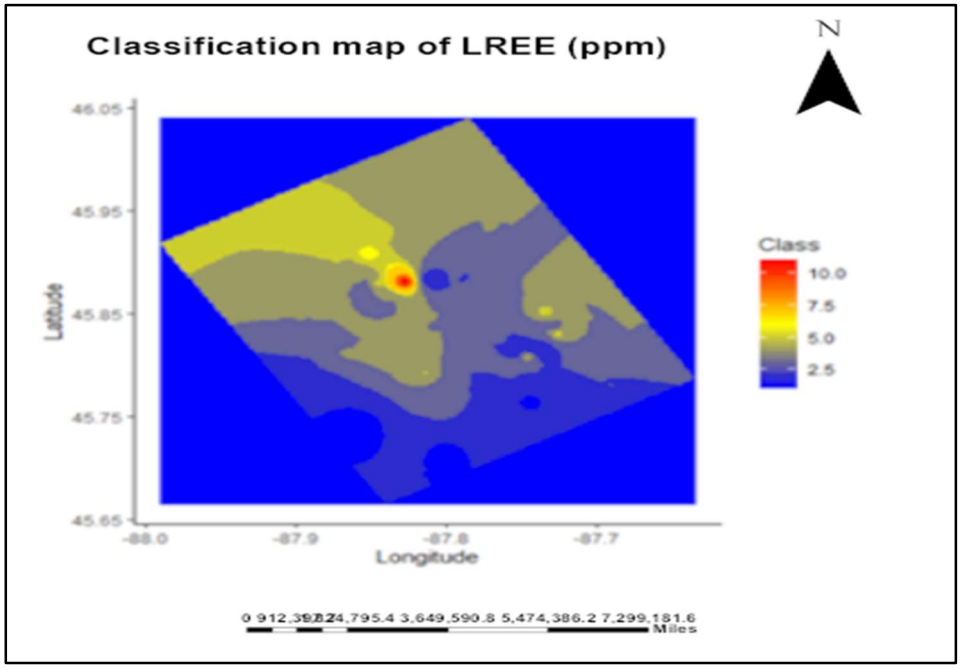

Figure 1. 27 Classification map of LREEs.

The classification map displays the spatial distribution of LREEs concentrations in parts per million (ppm) within a specified geographic region. Shown in Figure 1.27 is the classification map of LREEs, and the color gradient spans from blue to red, indicating escalating levels of LREEs concentrations. Blue regions denote the background areas with the lowest LREEs concentrations (class 2.5 and below), while green to yellow regions imply moderate anomalies (class 5 to 7.5). Red zones highlight the most substantial anomalies (class 10), which may potentially indicate the presence of mineralization. Similarly, for the HREEs, the distribution of anomalies on the anomaly map implies a non-homogeneous spread, where concentrations are probably impacted by the geological structures and processes beneath. The anomaly map in Figure 1.28 illustrates the existence of specific areas with notably elevated levels of HREEs, notably in the southwest region. It demonstrates a noticeable contrast between regions presenting a greater likelihood for economic mineral deposits (identified by red and orange zones) and those with lower potential (highlighted by yellow and green zones). Areas with concentration levels between 53.172-71.573 ppm have very high anomalies.

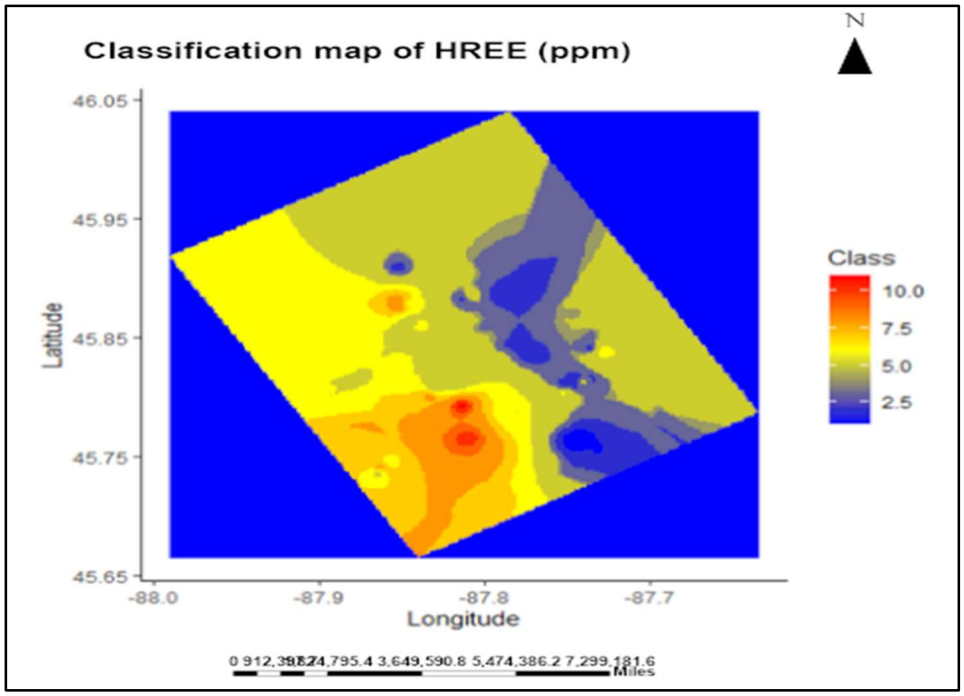

Figure 1. 28 Classification map of HREEs.

HREEs distributions were mapped using only the geochemical data on one hand and with geophysical data (gravity and magnetic) on the other hand as supplementary information sources. Below is the comparison of the various maps generated. Figures 1.29 and 1.30 show the classification maps of LREEs with and without the gravity and magnetic data. When supplementary geophysical data are not used, the geochemical map shows an unusual geochemical signature of HREEs, mostly in the southern sector of the area under study. A chromatic gradient is utilized to quantitatively depict this anomaly, wherein the red color corresponds to the highest concentrations. It is indicative of geochemical halos resulting from secondary enrichment, weathering, hydrothermal alteration, and fluid migration that the geochemical distribution displays a zonal gradation of concentration levels. Similarly, Figures 1.29 and 1.30 highlight the difference in the classification maps of HREEs using only geochemical data and when integrated with gravity and magnetic data.

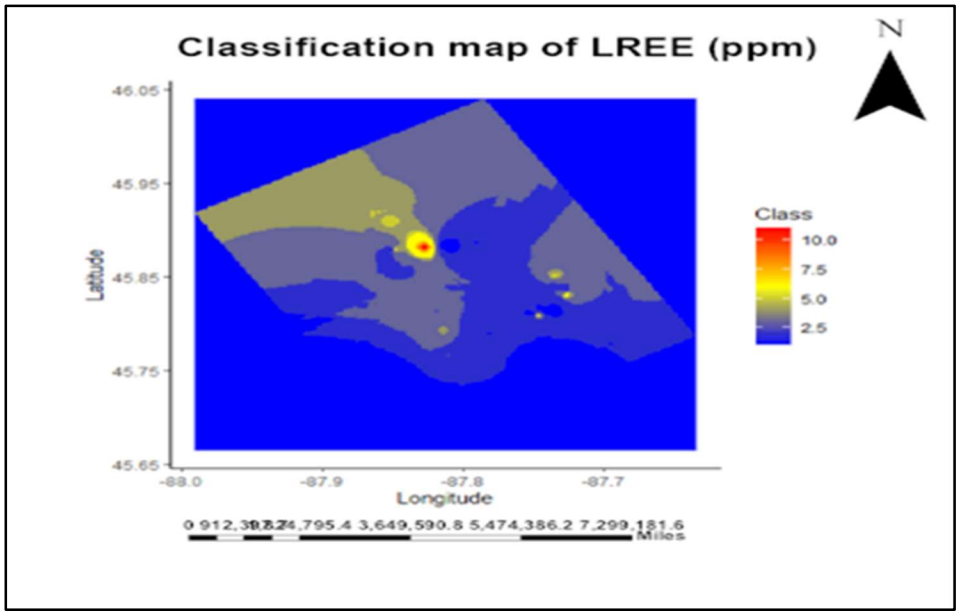

Figure 1. 29 Classification maps of LREEs using geochemical data.

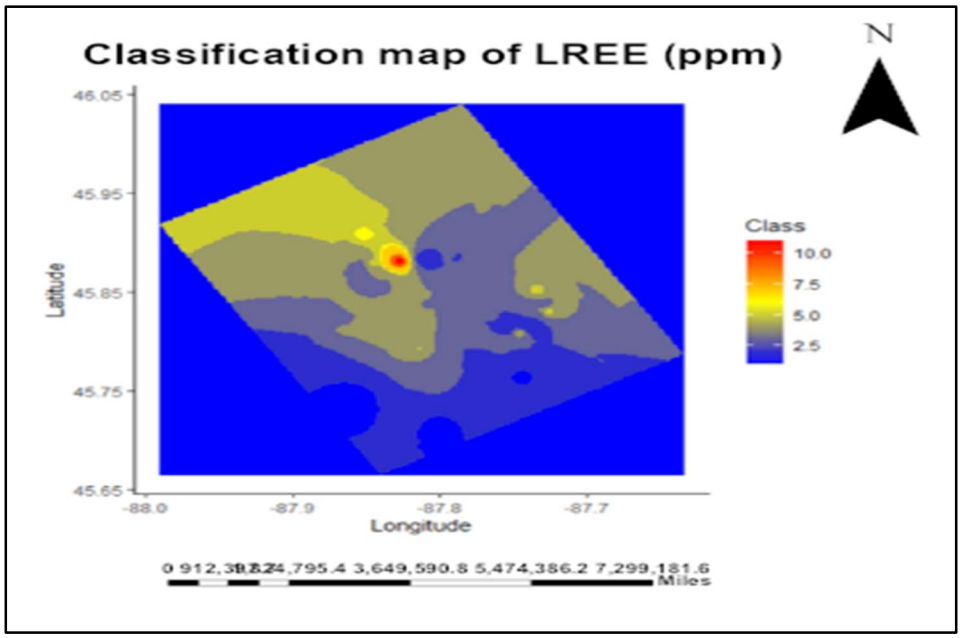

Figure 1. 30 Classification maps of LREEs using geochemical data with geophysical data.

Conversely, in the combined map shown in Figures 1.31 and 1.32 integrating gravity and magnetic data with geochemical information reveals a more precise and concentrated layout of high HREEs concentration zones. The inclusion of gravity data aids in comprehending variations in subsurface density, often linked to mineral deposits, while magnetic data can signal the presence of magnetic minerals frequently associated with

specific types of HREEs mineralization. The map anomalies are more distinctly defined, indicating that incorporating gravity and magnetic data provides enhanced clarity regarding the presence of dense, mineral-laden formations below the Earth's surface. In summation, the consolidated map, which includes geochemical, gravity, and magnetic data, presents a more sharpened and potentially accurate representation of the subsurface concentrations of HREEs, guiding exploratory initiatives to the zones with the highest potential for economical mineral extraction.

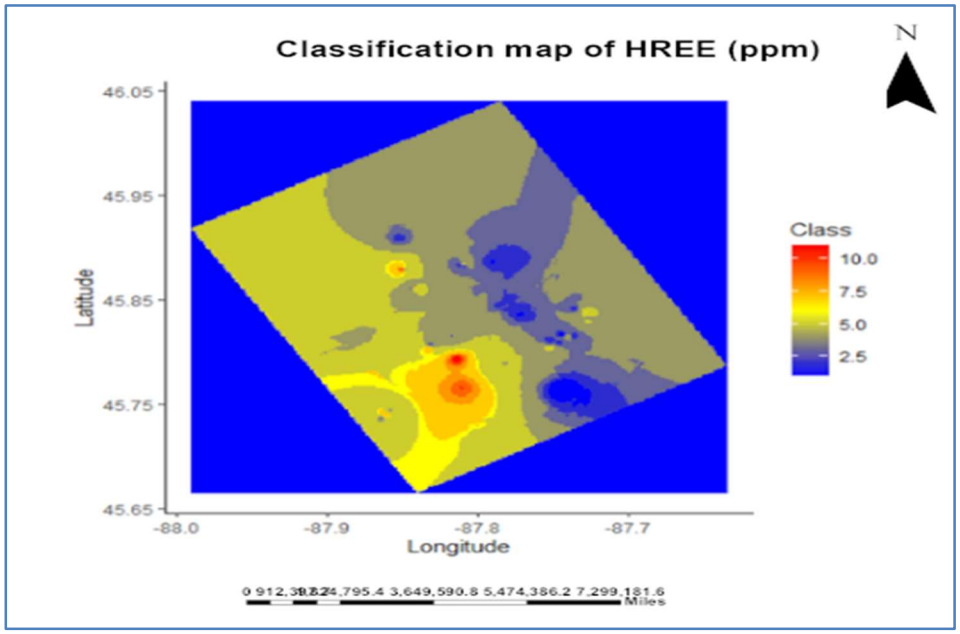

Figure 1. 31 Classification map of HREEs using geochemical data.

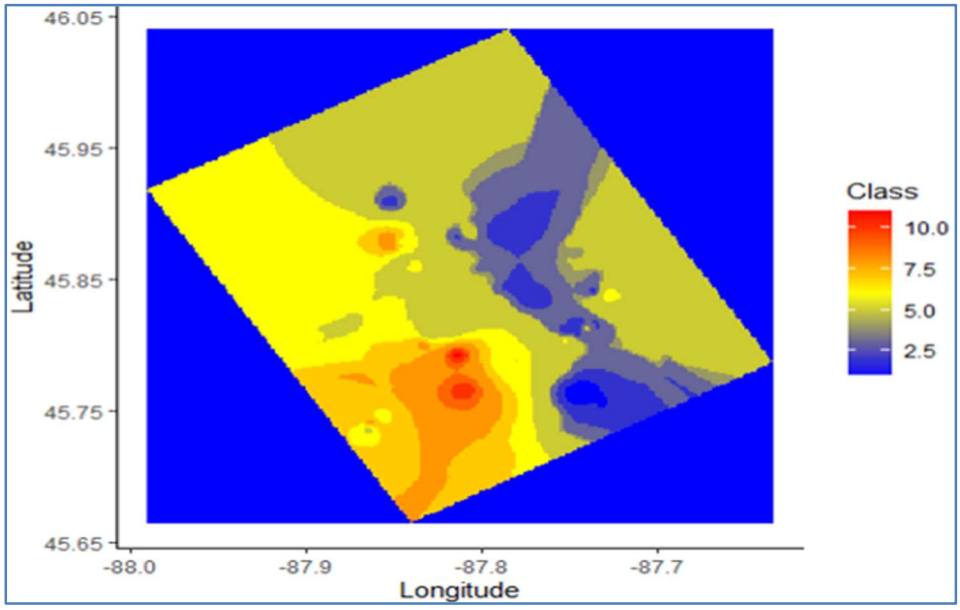

Figure 1. 32 Classification map of HREEs using geochemical data with geophysical data.

5 Conclusion

Based on the findings obtained through analysis of the C–A fractal model and the log-log plots of gravity, magnetic, and geochemical data, notable concentration anomalies of HREEs fall within the range of 53.172-71.573 ppm, while for LREEs, the range is from 260.3 to 461.9. The study highlights the effectiveness of utilizing a multidisciplinary geoscientific approach to enhance the accuracy and resolution of anomaly mapping of LREEs and HREEs. Empirical findings indicate that merging geochemical profiles with geophysical data, particularly gravity and magnetic surveys, significantly improves the identification of subsurface mineralized zones. This combined method helps overcome the limitations of using isolated geochemical data, which mainly reflect surface mineral occurrences and can be altered by weathering processes. Utilizing gravity measurements adds a crucial aspect to this integrated approach by aiding in identifying density differences that point to ore bodies beneath the Earth's surface. Magnetic data complements this by outlining anomalies related to the magnetic characteristics of geological formations, often linked to mineralization. By merging these datasets, more precise and geologically coherent anomaly patterns can be identified compared to using single-discipline exploration methods.

Through leveraging the strengths of each geoscientific technique, the study demonstrates that the composite data model offers a more precise spatial depiction of potential LREEs and HREEs deposits. The resulting anomaly maps show improved clarity and specificity, enabling a more targeted exploration approach. Furthermore, this integrated model provides insights into the three-dimensional layout of anomalies, enhancing the understanding of the region's geological framework.

In conclusion, the empirical data from this study supports the use of an integrated approach as a best practice in the search for economically viable concentrations of LREEs and HREEs. The integration of geochemical, gravity, and magnetic data not only enhances the direct identification of anomalies but also enriches the geological interpretation of the subsurface context, crucial for prioritizing exploration targets. The study's results advocate for this comprehensive methodology to become a standard procedure in mineral exploration, ensuring a more efficient allocation of exploration resources and optimized prospectivity evaluations.

6 Reference List

Afzal, P., Khakzad, A., Maarefvand, P., Rashidnejad Omron, N., Esfandiari, B., & Fadakar Alghalandis, Y. (2010). Geochemical anomaly separation by multi-fractal modeling in Kahang (Gor Gor) porphyry system, Central Iran. Journal of Geochemical Exploration, 104, 34-46.

African Natural Resources Centre (ANRC). 2021. Rare Earth Elements (REE). Value Chain Analysis for Mineral Based Industrialization in Africa. African Development Bank. Abidjan, Côte d'Ivoire.

Bai, J., Porwal, A., Hart, C., Ford, A., & Yu, L. (2010). Mapping geochemical singularity using multifractal analysis: Application to anomaly definition on stream sediments data from Funin Sheet, Yunnan, China. *Journal of Geochemical Exploration*, 104(1-2), 1-11. https://doi.org/10.1016/j.gexplo.2009.09.002

Balaram, V. (2019). Rare earth elements: A review of applications, occurrence, exploration, analysis, recycling, and environmental impact. *Geoscience Frontiers*, 10(4), 1285-1303. https://doi.org/10.1016/j.gsf.2018.12.005

Bedini, E. (2017). The use of hyperspectral remote sensing for mineral exploration: A review. Journal of Hyperspectral Remote Sensing, 7(4), 189-211. https://doi.org/10.29150/jhrs.v7.4.p189-211

Calam, C. (2023, February 5). Can You Name All 17 Rare Earth Elements? ThermoFisher Scientific. Retrieved from https://www.thermofisher.com/blog/mining/can-you-name-all-17-rare-earth-elements/

Chen W, Honghui H, Bai T, Jiang S. Geochemistry of Monazite within Carbonatite Related REE Deposits. Resources. 2017; 6(4):51https://doi.org/10.3390/resources6040051

Emsbo, P., McLaughlin, P. I., Breit, G. N., du Bray, E. A., & Koenig, A. E. (2014). Rare earth elements in sedimentary phosphate deposits: Solution to the global REE crisis? Gondwana Research, 27(3), 776-785. https://doi.org/10.1016/j.gr.2014.10.004

ESRI. (n.d.). *Set Null (Spatial Analyst)*. ArcGIS Pro 3.2. Retrieved on April 15th, 2024 from https://pro.arcgis.com/en/pro-app/latest/tool-reference/spatial-analyst/set-null.htm

Farahbakhsh, E., Maughan, J., & Müller, R. D. (2023). Prospectivity modelling of critical mineral deposits using a generative adversarial network with oversampling and positive-unlabelled bagging. *Ore Geology Reviews*, 105665. https://doi.org/10.1016/j.oregeorev.2023.105665

Heidari, S. M., Ghaderi, M., & Afzal, P. (2013). Delineating mineralized phases based on litho-geochemical data using multi-fractal model in Touzlar epithermal Au-Ag (Cu) deposit, NW Iran. Applied Geochemistry, 31, 119-132.

Khalajmasoumi, M., Sadeghi, B., Carranza, E. J. M., & Sadeghi, M. (2017). Geochemical anomaly recognition of rare earth elements using multi-fractal modeling correlated with geological features, Central Iran. *Journal of Geochemical Exploration*, **172**, 44-54. https://doi.org/10.1016/j.gexplo.2016.12.011

King, H. M. (n.d.). REE - Rare Earth Elements and their Uses. Retrieved April 17, 2024 from https://geology.com/articles/rare-earth-elements/

Long, K. R., Van Gosen, B. S., Foley, N. K., & Cordier, D. (2010). The Principal Rare Earth Elements Deposits of the United States: A Summary of Domestic Deposits and a Global Perspective. https://doi.org/10.1007/978-90-481-8679-2_7

Nazari Ostad, M., Emami Niri, M., & Darjani, M. (2018). 3D modeling of geomechanical elastic properties in a carbonate-sandstone reservoir: A comparative study of geostatistical co-simulation methods. *Journal of Geophysics and Engineering, 15*(4), 1419–1431. https://doi.org/10.1088/1742-2140/aaa983

Parker, B.K. (1987). *Rare earth and related elements in the Goodrich Quartzite, Marquette County, Michigan.* Michigan Geological Survey Division, Department of Natural Resources. Open File Report OFR 81-2.

Reitman, J.J., Drenth, B.J., and Anderson, E.D., 2020, Principal facts of regional gravity data in the central Upper Peninsula, Michigan, and northeastern Wisconsin: U.S. Geological Survey data release, https://doi.org/10.5066/P9IATNBD. https://www.sciencebase.gov/catalog/item/5f039bda82ce0afb2446e102

United States Geological Survey. (2018, October 24). *Airborne magnetic total-field survey: Northern Michigan, USA.* USGS. Montréal, Québec, Canada.

Van Gosen, B.S., Verplanck, P.L., Seal, R.R., II, Long, K.R., and Gambogi, Joseph, 2017, Rare-earth elements, chap. O of Schulz, K.J., DeYoung, J.H., Jr., Seal, R.R., II, and Bradley, D.C., eds., Critical mineral resources of the United States—Economic and environmental geology and prospects for future supply: U.S. Geological Survey Professional Paper 1802, p. O1–O31, https://doi.org/10.3133/pp1802O.

Virginia Department of Energy. (n.d.). *Rare Earth Elements*. Retrieved from https://energy.virginia.gov/geology/REE.shtml

A Copyright documentation

Figure 1. 331 Jenkins, J. A., Musgrove, M., & White, S. J. O. (2023). Outlining potential biomarkers of exposure and effect to critical minerals: Nutritionally essential trace elements and the rare earth elements. Toxics, 11(2), 188. https://doi.org/10.3390/toxics11020188 Accessed March 2024. Accessed April 2024.

Table 1. 341 United States Geological Survey. (2018, October 24). Airborne magnetic total-field survey: Northern Michigan, USA. USGS. Montréal, Québec, Canada. Accessed December 2023.